Holocene history of 79°N ice shelf reconstructed from epishelf lake and uplifted glacimarine sediments

James A. Smith[1], Louise Callard[2], Michael J. Bentley[3], Stewart S.R. Jamieson[3], Maria Luisa Sánchez-Montes[4], Timothy P. Lane[5], Jeremy M. Lloyd[3], Erin L. McClymont[3], Christopher M. Darvill[6], Brice R. Rea[7], Colm O'Cofaigh[3], Pauline Gulliver[8], Werner Ehrmann[9], Richard S. Jones[10], David H. Roberts[3].

[1]British Antarctic Survey, High Cross, Madingley Road, Cambridge, CB3 0ET, UK.

[2]School of Geography, Politics and Sociology, Newcastle University, Newcastle upon Tyne, NE1 7RU, UK.

[3]Department of Geography, Durham University, Durham, DH1 3LE, UK.

[4]INSTAAR – Institute of Arctic and Alpine Research, University of Colorado Boulder, Boulder, CO 80309-0450, USA.

[5]School of Biological and Environmental Sciences, Liverpool John Moores University, Liverpool, L3 3AF, UK.

[6]Department of Geography, University of Manchester, Manchester, M13 9PL, UK.

[7]School of Geosciences University of Aberdeen, Aberdeen, AB24 3TU, UK.

[8]NERC Radiocarbon Facility, East Kilbride, G75 0QF, UK.

[9]Institute for Geophysics & Geology, University of Leipzig, Leipzig 04103, Germany.

[10]School of Earth Atmosphere and Environment, Monash University, Clayton, Victoria, Australia.

Correspondence to: James A. Smith (jaas@bas.ac.uk)

Abstract. Nioghalvfjerdsbrae, or 79°N Glacier, is the largest marine-terminating glacier draining Northeast Greenland Ice Stream (NEGIS). In recent years, it's ~70km-long fringing ice shelf (hereafter referred to as 79°N ice shelf) has thinned, and a number of small calving events highlight its sensitivity to climate warming. With the continued retreat of 79°N ice shelf and the potential for accelerated discharge from NEGIS, which drains 16% of the Greenland Ice Sheet (GrIS), it has become increasingly important to understand the long-term history of the ice shelf in order to put the recent changes into perspective and to judge their long-term significance. Here we reconstruct the Holocene dynamics of 79°N ice shelf by combining radiocarbon dating of marine mollusc from isostatically uplifted glacimarine sediments with a multi-proxy investigation of two sediment cores recovered from Blåsø, a large epishelf lake 2-13 km from the current grounding line of 79°N Glacier. Our reconstructions suggest that the ice shelf retreated between 8.5 and 4.4 cal. ka. BP, which is consistent with previous work charting grounding line and ice shelf retreat to the coast, and open marine conditions in Nioghalvfjerdsbrae. Ice shelf retreat followed a period of enhanced atmospheric and ocean warming in the Early Holocene. Based on our detailed sedimentological, microfaunal and biomarker evidence the ice shelf reformed at Blåsø after 4.4 cal. ka BP, reaching a thickness similar to present by 4.0 cal. ka BP. Reformation of the ice shelf coincides with decreasing atmospheric temperatures, increased dominance of Polar Water, a reduction in Atlantic Water and (near) perennial sea-ice cover on the adjacent continental shelf. Together with available climate archives our data

indicate that 79°N ice shelf is susceptible to collapse when mean atmospheric and ocean temperatures are ~2°C warmer than present, which could be achieved by the middle of this century under some ~~climate model~~emissions scenarios. Finally, the presence of 'marine' markers in the uppermost part of the Blåsø sediment cores could record modern ice shelf thinning, although the significance and precise timing of these changes requires further work.

1 Introduction

The GrIS is losing mass at an accelerating rate and is currently the largest single contributor to global sea level rise (Oppenheimer et al., 2019). Model projections suggest that mass loss will continue to accelerate in a warming climate, with the potential for ~7.4 m of sea level rise (Morlighem et al., 2017; Aschwanden et al., 2019). Mass loss has been driven by increases in atmospheric (Fettweis et al., 2017; Hanna et al., 2021) and ocean (Straneo and Heimbach, 2013; Wood et al., 2021) warming, which has resulted in enhanced melting of both the ice sheet surface and the undersides of marine terminating glaciers, respectively. Despite an improved understanding of the drivers of recent mass loss, the short time-span of the observational record provides a limited time-series with which to understand the complex, and often non-linear, response of the margins of the GrIS to climate forcing (Nick et al., 2010). This restricts our ability to reliably forecast how ice sheets will evolve in the future (Seroussi et al., 2013). In this context, reconstructions of past ice sheet responses to atmospheric and ocean-driven forcing can be used to validate and test the sensitivity of predictive models. In turn, this can lead to a better understanding of the feedbacks that amplify or dampen mass loss and whether tipping points exist, beyond which retreat is irreversible (Aschwanden et al., 2019).

79°N Glacier is the largest of three marine-terminating glaciers of the NEGIS (Fig. 1) and contains enough ice to raise global sea level by 0.57 m (An et al., 2021). Until recently, 79°N Glacier was assumed to be relatively stable (Joughin et al., 2010), but recent observations indicate increasing surface velocities and glacier thinning (Khan et al., 2014; Mayer et al., 2018; An et al., 2021). Mass loss has occurred as several small calving events at the ice shelf margin, equating to a ~4% reduction in the total area of the ice shelf between 1999 and 2013 (Blau et al., 2021). During approximately the same period (1998-2016), the ice shelf has lost one third of its thickness in the region of the Midgårdsormen Ridge (Mayer et al., 2018), ~5km downstream of the grounding line (Fig. 1). These changes are thought to have been driven by both atmospheric and ocean warming. The circulation of relatively warm Atlantic Water beneath the ice shelf (Schaffer et al., 2020), which likely penetrates all the way to the grounding line (Bentley et al., 2022), is driving basal melt rates of ~10 m a^{-1}. Average air-temperatures have also increased by ~3°C during the past 40 years (Turton et al., 2021), with supraglacial melt lakes now a persistent feature (Leeson et al., 2015; Hochreuther et al., 2021). Given that further retreat is predicted following the break-up of Spalte Glacier (a northern tributary of the 79°N ~~Glacier~~ice shelf; Fig. 1) in 2019 and 2020, which could activate further dynamical thinning and acceleration of the NEGIS drainage basin (Khan et al., 2014; Choi et al., 2017), it has become increasingly important to understand the long-term dynamics of the ice shelf in order to contextualise the recent changes.

Based on [10]Be surface exposures ages, the deglaciation of Nioghalvfjerdsfjorden occurred between 9.2 and 7.9 ka (Larsen et al., 2018). This concurs with earlier work dating whale bones and other macro-fossils along the margins of 79°N ice shelf, which indicated that it retreated inboard of the current location during the Holocene Thermal

80   Maximum (HTM; ~8.0-5.0 cal. ka BP) (Bennike and Weidick, 2001), when atmospheric temperatures were elevated above present. Ocean warming and reduced sea-ice have also been documented to the east of 79°N in the Early Holocene (Werner et al., 2016; Syring et al., 2020; Pados-Dibattista et al., 2022) suggesting that ice shelf retreat was driven by both atmospheric and ocean forcing. In this paper we utilise chronologically constrained lacustrine sediment cores recovered from the northern margin of the ice shelf and combine these with new and

85   existing (Bennike and Weidick, 2001; Larsen et al., 2018) age-control from uplifted glacimarine deposits to provide a detailed Holocene history of 79°N ice shelf. We discuss these results in the context of both atmospheric and oceanic warming, which in the past forced ice shelf retreat, and use this to contextualise changes due to ongoing climate warming.

2 Study area and approach

90

Blåsø is a large epishelf lake located at sea-level on the northern margin of 79°N Glacier (Fig. 2). It is located within the East Greenland Caledonides, a series of W-directed thrust sheets displaced against the rocks of the Palaeo- to Mesoproterozoic foreland (Higgins and Kalsbeek, 2004). The crystalline basement, consisting of strongly deformed Archaean and Palaeoproterozoic granitoid rocks, is overlain by Mesoproterozoic-

95   Neoproterozoic and lower Palaeozoic strata. To the east of Blåsø, outcrops of quartzite/sandstones (Hovgaard Ø Formation), dolerites and flood basalts (Midsommersøte Dolerite Formation) are exposed. Moving westwards these are overlain by the Neoproterozoic Rivieradal Group consisting of conglomerate, sandstone turbidite and mudstone units (Smith et al., 2004a). In turn, these are overlain by the limestones, mudstones and dolomites of the Odins Fjord, Turesø and Børglum River formations further west (Smith et al., 2004b). The n-shape lake abuts

100   the ice shelf at two locations, approximately 2 and 13 km from the grounding line of 79°N Glacier. Blåsø has a well-resolved tidal signal and is stratified. At its eastern end, where the deepest water has been documented (Bentley et al., 2022), freshwater to brackish water 145 m-thick, overlies a warm (<0.7 °C) marine layer, sourced from modified Atlantic Water which flows beneath the ice shelf and into and out of the lake driven by the local tides. The halocline at 145 m acts as a proxy for the draught of the floating tongue of 79°N at the eastern margin,

105   assuming the ice is in hydrostatic equilibrium (Bentley et al., 2022). While marine water is only detected at the eastern margin, there is observational evidence to suggest that periodically the western margin connects to the sub-shelf cavity allowing small volumes of marine water to mix into the western part of the lake (e.g. sub-ice-shelf fish species observed in the lake; Bentley et al., in prep2022). The present-day limnology of Blåsø, and therefore its concomitant sedimentary signature, is controlled by the 79°N ice shelf 'dam', without which, the lake

110   would become a marine embayment (see Figure Fig. 10 in Smith et al. (2006)). The sedimentary records deposited within epishelf lakes can therefore provide continuous archives of past ice-shelf dynamics (Smith et al., 2006). For example epishelf lakes in Antarctica and the Canadian Arctic have yielded detailed ice shelf histories, including information on the timing of ice shelf collapse and reformation as well as the elucidating the drivers of change from biological and geochemical proxies contained within the lake sediments (Bentley et al., 2005; Smith

115   et al., 2007; Antoniades et al., 2011). Proximal to Blåsø, uplifted glacimarine sediments around the lake can be

found up to 40 m above sea-level (m.a.s.l) (Bennike and Weidick, 2001). These sediments were linked to a period of ice shelf absence during the Early Holocene, but they have not been analysed in detail, nor related to the adjacent epishelf lake sediments. By investigating the lacustrine and uplifted marine sediments in combination, a detailed history of 79°N ice shelf is reconstructed.

3 Methods

3.1 Core recovery and sampling of uplifted glacimarine sediments

Fieldwork was carried out between 19th July and 11th August 2017~~in the austral summer of 2017~~ when, with the exception of the far eastern end of the lake which abuts 79°N ice shelf, Blåsø was largely ice-free. Following detailed bathymetric survey (Bentley et al., 2022), coring was focussed within an ~90-100 m-deep 'central' basin (Fig. 2) where sub-bottom profiler data showed stratified sediments up to ~20 m in thickness (Fig. 3). Core sites LC7 (87 m water depth; 79°35.340, 22°29.640) and LC12 (90 m water depth; 79°35.688, 22°26.540) targeted the thinner drape at the edge of the basin infill (Fig. 3) to ensure the longest (temporal) record was recovered. An additional advantage of coring the central basin is that it is currently isolated from marine water since the ice shelf draft - in its current configuration~~s~~ - is sufficient to block marine water from filling the entire basin (Bentley et al., 2022). Detection of marine markers in the sedimentary record at this site would present clear evidence for a significantly thinner than present or entirely absent ice shelf. Furthermore, the central basin is sufficiently distal from the glacially fed rivers entering the north-western side of the lake, thereby avoiding excessive coarse sediment inputs (observed during fieldwork) which could overprint the paleoenvironmental record.

Overlapping 2 m-long sediment cores were recovered with a UWITEC KOL 'Kolbenlot' percussion piston corer to a total sediment depth of 3.74 m (LC7) and 5.24 m (LC12). Coring was performed from a UWITEC raft, fitted with a 15-horsepower Yamaha outboard. Multi-proxy analyses (below) were performed on both cores, with particular focus on 'marine' lithofacies (LF1) identified in LC7 and LC12. Additional analyses (clay mineral, biomarkers) were performed on LC12 because it recovered the longer sequence so was prioritised as the 'master core'.

Uplilfted glacimarine sediments were described following standard sedimentological procedures (Evans and Benn, 2004). In-situ mollusc (*Hiatella Arctica*) and gastropods were recovered from the uplifted glacimarine sediment at various locations above the western shore of Blåsø, 0-up to 40 m.a.s.l (Fig. 2). Only articulated shells were collected and dated. The altitude was measured by handheld GPS units. Uplifted glacimarine sediments and push ridges were also surveyed using a theodolite from base (lake) level. Foraminifera are also present in the uplifted marine sediment but were only assessed qualitatively.

3.2 Sedimentological, physical properties and geochemical analyses

Physical properties (magnetic susceptibility, wet bulk density) and X-radiographs were measured on whole core using a GEOTEK multi-sensor core logger (MSCL) and GEOTEK X-ray CT Core Imaging System (MSCL-XCT) respectively, at the Department of Geography, Durham University, to characterise lithological properties and infer

the depositional environment(s). Core sections were then split, described and sub-sampled. 1-cm thick sediment slices were taken every 10-20 cm. Grain-size analyses was performed on core LC12 using a Beckman Coulter LS 13 320 Laser Diffraction particle size analyser. Prior to analysis sediment samples were treated with 20% hydrogen peroxide to digest the organic material. Once the organic material has had been digested the sample was centrifuged and then 20 ml distilled water plus 2 ml, 35% sodium hexametaphosphate was added to disaggregate deflocculate the sample. High-resolution elemental abundances were measured on the split core using a GEOTEK X-ray Fluorescence (MSCL-XRF) at 1 mm resolution. We use elemental ratios Ti/Ca as a proxy for terrigenous flux source variations (i.e., siliciclastic vs. carbonate rocks), while Mn/Fe and Br concentrations provides semi-quantitative information about lake oxygenation (Naeher et al., 2013) and marine organic carbon content (Ziegler et al., 2008) respectively. Ti contents in marine sediments is are directly linked to terrigenous (siliciclastic) sediment supply delivered by fluvial and/or aeolian transport processes (Arz et al., 1999; Nace et al., 2014), while Ca concentrations reflect changes in the production of calcium carbonate ($CaCO_3$) by marine plankton (Bahr et al., 2005). High Ti/Ca ratios are indicative of an increased terrigenous flux. The behaviour of Fe and Mn is strongly dependent on processes of oxidation and reduction. Reducing conditions are the result of O_2 consumption during organic matter (OM) remineralisation, which releases Fe and Mn. Because Fe oxidises faster than Mn, high Mn accumulation and thus high(low) Mn/Fe ratios reflect oxic(anoxic) conditions. Bromine (Br) is used as a proxy for marine organic carbon, since bromine is found at higher concentrations in marine, compared to terrestrial, organic matter (Ziegler et al., 2008; Seki et al., 2019). Finally, an aliquot of the ≤ 2 μm fraction was used to determine the relative concentrations of the clay minerals smectite, illite, chlorite and kaolinite in LC12 using an automated powder diffractometer system (Rigaku MiniFlex) with CoKα radiation (30 kV, 15 mA) at the Institute for Geophysics and Geology (University of Leipzig, Germany). The clay mineral identification and quantification followed standard X-ray diffraction methods (Ehrmann et al., 2011) and is used to reconstruct sediment provenance and pathways. Illite/chlorite are detrital clay minerals which are typically derived from physical weathering of crystalline/basement rocks i.e., granitoids and low-grade, chlorite-bearing metamorphic and basic rocks i.e., dolerites, respectively. Smectite normally reflects volcanic sources i.e., basalts and volcanic glass, whilst kaolinite is a product of chemical weathering, characteristic of moist, temperate to tropical regions. Kaolinite generally indicates the presence of older sedimentary strata i.e., mudstones/shales.

3.3 Foraminiferal analysis

A total of 16 (LC12) and 6 (LC7) samples were processed for foraminiferal analysis to reconstruct the environmental conditions in Blåsø. Sample volume varied between 0.5 and 5 ml (cm^3) depending on average foraminiferal concentration (estimated based on initial scanning of samples). The variation in sample size was designed to allow ~300 to 500 specimens to be counted from all samples. Once extracted samples were soaked in deionized water for several hours to help disaggregate the sediment. Samples were then washed through a 500 μm and 63 μm mesh sieve to concentrate the foraminifera. The material collected on the 63 μm mesh sieve were retained for foraminiferal analysis. Foraminifera were identified and counted from the wet (non-buffered) residue under a binocular microscope.

3.4 Lipid biomarker extraction and analyses

A total of 22 sediment samples from LC12 were prepared for lipid biomarker analyses. Lipids were microwave-extracted from 0.4 to 2g of freeze-dried and homogenised sediment were extracted using dichloromethane:methanol (3:1) at an oven temperature of 70°C for two minutes following Kornilova and Rosell-Melé (2003). Internal standards of known concentration (5α-cholestane, Heptatriacontane and 2 nonadecanone) were added to aid quantification. The extracted sediment was centrifuged at 2,500rpm for 5 minutes. The solvent was decanted and then taken to near-dryness with a stream of N_2. The total lipid extract was separated into 3 fractions using glass Pasteur pipettes packed with extracted cotton wool and a 4 cm silica column (high purity grade pore size 60Å 220-440 mesh particle size, 35-75μm particle size for flash chromatography, ©Sigma Aldrich, size of particles). Sequential elution with Hexane, Dichloromethane and Methanol (4 columns each) yielded *n* - alkane, ketone and polar fractions, respectively.

Biomarkers were quantified and identified using gas chromatography with flame ionisation (GC-FID) and mass spectrometry (GC-MS) as outlined in detail in Sánchez-Montes et al. (2020). The internal standards were used to calculate lipid mass, normalised to the original extracted dry weight of sediment. We employ a range of *n*-alkanes and ketones as environmental proxies, using a series of equations used to determine the relative contribution of bacteria, and phytoplankton and grasses to sediments, as well as indicators of water temperature and salinity (Table 1). The terrigenous and aquatic OM equations in Table 1 were normalised to the weight of the sediment extracted. Also, because Blåsø has experienced both marine (LF1) and lacustrine (LF2-3) conditions, the alkenone U^K_{37} index was converted into surface water temperature (SWT) using both the surface temperature calibration equation of D'Andrea et al., (2011), which was developed for lakes in West Greenland, and the marine temperature calibration in Bendle and Rosell-Melé, (2004) developed for the Nordic Seas (Table 1).

3.5 Core chronology

The chronology for LC7 and LC12 was established using accelerator mass spectrometry (AMS) radiocarbon (^{14}C) dating. Where possible, calcareous microfossils (mixed benthic foraminifera) were dated, and bulk (acid insoluble organic matter AIOM)) sediment was only dated in the absence of microfossils. To assess the reliability of the AIOM fraction, we also performed 'paired' foraminifera and AIOM dating on two horizons (~297 cm and 327 cm). Cores were also inspected for other datable macrofossils (mosses, algae, shells) but were found to be barren. ^{14}C dating of samples from the lake cores, together with macro-fossils (molluscs, gastropods) from the raised marine deposits, was undertaken at the NERC Radiocarbon Laboratory (Environment) in East Kilbride, UK (SUERC-), the Keck-CCAMS, University of California, Irvine, US (UCIAMS-) and Beta Analytic, Miami, US (BETA-). Radiocarbon ages were calibrated to calendar years before present (cal. years BP, where present is A.D. 1950) using the calibration software CALIB 8.1.0 (Stuiver et al., 2021), the Marine13 Marine20 calibration curve (Heaton et al., 2020) , and and a a marine reservoir of 550 years (ΔR = of 1500±0 years) following Hansen et al. (2022) . The Marine20 calibration was not used owing to its unsuitability for sea ice dominated polar environments . Marine20 estimates an increase in the (globally-averaged) marine reservoir age compared to Marine13, ranging from ~550-410 ^{14}C years for the pre-bomb period. This is ~150 years older than the marine reservoir age in Marine13, which was 405 ^{14}C years (Reimer et al., 2013). Thus a ΔR of 0±0 years, as advocated by Hansen et al. (2022), essentially replicates previously published work from the region using Marine13 e.g. ΔR

150±0 years (Larsen et al. 2018), and results in near-identical calibrated ages. A ΔR of 0±0 years is also very similar to the geographically nearest data point to 79°N in the Marine20 marine reservoir database (Map. No. 31 = ΔR 3±60 years; Funder, 1982). However, as outlined in O'Regan (2020), the absence of *a priori* information regarding local marine reservoir corrections for many areas of Greenland could result in a broad envelope of uncertainty in calibrated ages. Unfortunately, without additional work, including the use of independent dating techniques i.e., relative paleointensity, it remains difficult to fully quantify this. For example, variations in sea ice cover, different water masses or input of glacial meltwater, all have the potential to impact the local marine reservoir age (see O'Regan et al., 2020; Pados-Dibattista et al., 2022; Hansen et al., 2022; Heaton et al., 2022 for further discussion).

4 Results and interpretation

4.1 Blåsø

LC7 consists of two overlapping ~2-m long cores with a composite core recovery of 3.74 m. LC12 consists of three 2-m cores, although we only have confidence that the upper two drives overlap. The uncertain splice likely reflects movement of the raft during coring operations, with the third drive of the piston-corer penetrating a different part of the sediment drape. For this reason, we only present data for the upper two sections of LC12. Multi-proxy analyses reveal three main lithofacies (LF1-3) in LC12 and LC7 (Fig. 4, Fig. 5).

LF1: The lowermost sediments in both cores are generally brown, massive (LC12) to crudely stratified (LC7) clay/silts with occasional gravel and pebble-sized clasts (Fig. 6). Magnetic susceptibility increases to a peak at ~300 cm in LC12 before decreasing and decreases up-core in LC7 (Fig. 4, 5). LC12 shows an interval of increased coarse silt between 320 and 300 cm (Fig. 5). The clay mineral assemblage in LC12 is dominated by chlorite and illite with lower smectite and kaolinite contents (Fig. 7). XRF-scanning data shows a high degree of variability throughout both cores. LF1 is characterised by low Ti/Ca (0.01-0.05) and Mn/Fe values between 0.01 and 0.05. Br values are typically high (~20 cps) but decrease between ~320-305 cm in LC12.

Benthic foraminifera are present throughout LF1 (370.5-282 cm) in LC12 (Fig. 5), with the exception of one horizon at 314 cm, which was entirely barren. The ~~with an~~ assemblage is dominated by *Cassidulina reniforme* (>50%). *Elphidium ~~exavatum f. clavata~~clavatum* is also common (10-20%) together with *Stainforthia feylingi* (5-10%) and *Stetsonia horvathi* (variable but up to 15% below 300cm). There is a significant shift in fauna in the uppermost part of LF1 (290.5-282 cm) with *S. horvathi* becoming dominant (30 - >50%) while *C. reniforme* reduces, but is still very common (20-30%). *E. ~~excavatum f. clavata~~ clavatum* reduces in abundance to below 10% and *S. feylingi* increases slightly to >10%. This section is also characterised by a significant increase in foraminiferal concentration, with the uppermost sample (282 cm) having the highest foram per ml due to an increase in *S. horvathi*.

The faunal record from LC7 is very similar to LC12 (Fig. 4), although fewer samples were analysed. In total 6 samples were counted from 377 to 228 cm. Foraminifera disappear abruptly above 228 cm (LF1/LF2 boundary). The lower section (377 – 248 cm) is dominated by *C. reniforme* (60-75%) with *E. ~~excavatum f. clavata~~ clavatum*

275 (10-20%), *S. feylingi* <10% and *S. horvathi* <5% also common in decreasing importance. In the uppermost sample containing foraminifera (228 cm), the abundance of *S. horvathi* increases to >50%, *S. feylingi* remains common (approx. 10%) while *C. reniforme* decreases to 27%, and *E. ~~excavatum f. elavata~~ clavatum* decreases to <5%.

U^K_{37} typically displays high values (-0.1-0.1), with a minor decrease (-0.2) at 320 cm before increasing again (Fig.
280 8). The %$C_{37:4}$ mirrors the U^K_{37} with low concentrations (11 to 21%) and a peak of 25% at 320 cm. The K37/K38 index is variable (0.6-1.1), with a prominent peak (1.7-2.0) between 314 and 320 cm. The terrigenous (0.07-0.1 $\mu g\ g^{-1}$) and aquatic OM are typically low, the latter decreases up to 320 cm (from 0.5-0.2 $\mu g\ g^{-1}$) and remains low for the rest of LF1. The terrestrial to aquatic ratio (TAR) ~~and~~ C_{31}/C_{29} are variable but show a general increasing trend. The Pristane/Phytane and the carbon preference index (CPI) ratios display low values (1.2-1.8 and 0.7-1.0,
285 respectively).

Paleoenvironmental ~~i~~Interpretation: On the basis of abundant benthic foraminifera, high U^K_{37} and low %$C_{37:4,}$ indicative of relatively cool and saline water column (Bendle and Rosell-Mele, 2004), LF1 is interpreted to have been deposited in a seasonally-open marine setting. Specifically, the %$C_{37:4}$ values (10-25%) indicates absence,
290 or low concentrations (<30%), of sea-ice (Wang et al., 2021) and salinities similar to the North Atlantic close to the winter sea-ice edge (Wang et al., 2021). A corollary of this is that 79°N – the ice dam that currently prevents marine water from reaching the central basin of Blåsø – must have been absent at the time of deposition. The foraminiferal assemblage in the lowermost parts of LC12 and LC7 is dominated by *C. reniforme* (>50%), which is indicative of cold-water, typical of distal glacimarine conditions (Hald and Korsun, 1997; Slubowska et al.,
295 2005; Slubowska-Wodengen et al., 2007; Perner et al., 2011; Consolaro et al., 2018). *E. ~~excavatum f clavata~~ clavatum* is also common (10-20%) and has been associated with proximal to distal glacimarine conditions (Slubowska-Wodengen et al., 2007; Perner et al., 2011; Jennings et al., 2011). In contrast, the key Atlantic indicator species, *Cassidulina neoteretis* (Jennings et al., 2011; Jennings et al., 2004; Perner et al., 2015; Cage et al., 2021), occurs in low numbers with <5% abundance. Thus, the lowermost assemblage in LF1 indicates cold
300 glacimarine conditions, with minimal evidence for Atlantic-sourced waters. Above ~290 cm in LC12 and 228 cm in LC7 cold water indicators still dominate, but there is a significant increase in the abundance of *S. horvathi*. This species is commonly found associated with perennial sea ice cover (Wollenburg and Mackensen, 1998) and in some instances, below ice shelves (Jennings et al., 2020). Dominance of *S. horvathi* therefore suggests an increase in ice cover. An abrupt shift in alkenone producers between 300-314 cm (K37/K38) and a decrease in aquatic productivity (aquatic OM) below 300 cm also suggests a change in surface water properties (Fig. 8). Furthermore,
305 peaks in the K37/K38 index occur with higher %$C_{37:4}$ more closely compared to fresher North Pacific, rather than North Atlantic, waters suggesting ~~an~~ increased sea-ice concentration (Wang et al., 2021) and/or surface polar water influence (Bendle and Rosell-Melé, 2004) while still allowing aquatic algae productivity. The upper and lower foraminiferal assemblages in LC12 are separated by an increase in coarse silt, with corresponding peaks in
310 magnetic susceptibility, chlorite and K37/38 (Fig. 5, 7, 8). This interval either reflects a period of enhanced deposition of ice-rafted debris (IRD) within an ice-free marine embayment or the first sign of glacier advance associated with ice shelf reformation~~.~~ Generally, IRD-sized material (>125 um) is relatively rare throughout both cores which probably relates to the bathymetry of Blasø – and specifically ridges at both sides of the central basin (Fig. 2) which act to block large bergs reaching the core sites. ~~Coincident~~ Nevertheless, coincident with ~~an~~ the

315 increase in coarser detritus in LC12 we see a minor shift to colder/less saline water ($<U^K_{37}$; $>\%C_{37:4}$) (Prahl and Wakeham, 1987; Bendle and Rosell-Mele, 2004). We envisage that as the ice shelf started to ground at the eastern and western mouths of Blåsø, marine water was periodically restricted as fresher (lacustrine) conditions became more prevalent. Clay mineral data reveal information about sediment pathways linked to catchment geology. The Blåsø area comprises the northern part of the East Greenland Caledonides and the bedrock is primarily composed

320 of crystalline basement except for a few places on Lambert Land and north of Nioghalvfjerdsfjorden, where Palaeo-Mesoproterozoic sediments and basalts are present (Smith et al., 2004a). While high concentrations of illite likely reflects local input from the Rivieradal Group (Neoproterozoic sandstones/siliciclastic sediments primarily composed of quartz and feldspar grains together with small amounts of mica) and limestone bearing Odins Fjord Formation, the elevated chlorite content could reflect one of two sources, both of which require

325 absence of 79°N ice shelf. First, input from the basaltic rocks of Lambert Land (Fig. 1) to the south of Blåsø and second, input from crystalline basement which crops-out at the mouth of Nioghalvfjerdsfjorden on Hovgaard Ø (Fig. 1)(Smith et al., 2004a). Under both scenarios, absence of 79°N ice shelf would enable delivery of 'exotic' lithologies via iceberg rafting either across or down the length of Nioghalvfjerdsfjorden. Irrespective of the source, the overall clay mineral composition of LF1 (<smectite, >illite, and variable chlorite and kaolinite) is considered

330 as a 'marine' end-member.

LF2: This is a black, stratified to laminated mud (Fig. 6). Both grain-size and magnetic susceptibility decrease relative to LF1, while Ti/Ca ratios increase markedly (Fig. 4-6). Br values remain low and Mn/Fe values decrease and remain low. Smectite and kaolinite decrease with increases in illite and chlorite (Fig. 7). Foraminifera are

335 absent in LF2 although low numbers of chironomids (*Heterotrissocladius oliveri*-type) were observed.

A distinctive feature of LF2 is change in the alkenone GC profiles, evident in the highly variable ketone indices (Fig. 8). The U^K_{37} generally decreases compared to LF1 but is variable. Values peak at 274 cm (0.2), then decreases to -0.6 at 266 cm before increasing to -0.1 at 258 cm (Fig. 8). $\%C_{37:4}$ is anti-correlated with U^K_{37} with

340 low values at 274 cm (11%), peak values at 266 cm (67%) and lower values at 258 cm (24%). $\%C_{37:4}$ is generally higher relative to LF1. The variability of the K37/K38 index decreases compared to LF1 and remains between (0.8-1.0). In addition to the distinctive ketone indices, the terrigenous OM progressively increase up to a peak at 268 cm (0.27 μg g^{-1}), before decreasing to previous concentrations. The aquatic OM increases to 0.05 μg g^{-1} and then slowly decreases towards the top of LF2 (0.03 μg g^{-1}). The TAR and C_{31}/C_{29} continue being variable, both

345 peaking around 270 cm. The CPI and the Pristane/Phytane ratios remain low with values close to 1.

Paleoenvironmental iInterpretation: The absence of foraminifera, mix of alkenone producers (e.g., K37/K38; McClymont et al., 2005) coupled with an increase(decrease) in $\%C_{37:4}$(U^K_{37}), indicates a shift to a cold, less-saline environment (Bendle and Rosell-Mele, 2004). We attribute these changes to the isolation of Blåsø as 79°N ice

350 shelf reformed and grounded at the western and eastern margins. The shift from an exclusively marine (LF1) to a fresher, less saline water column occurs in steps, with the lowermost part of LF2 (280-274 cm) indicating that marine water still reached the core site and that the water column was well-mixed. In contrast above 274 cm, $\%C_{37:4}$ values imply a shift to a fresher water column and higher sea-ice concentrations.

Low Mn/Fe ratios, which also characterised the lower part of LF1 (Fig. 4, Fig. 5), indicates limited ventilation which we attribute to increases in lake ice (as inferred from $>\%C_{37:4}$), greater water-column stratification or a combination of both. Thicker lake ice would limit photosynthesis and exchange with the atmosphere, conditions that would be conducive to increased stratification and oxygen depletion. This is reflected in low Mn concentrations, indicative of Mn reduction under anoxic bottom water conditions. Anoxic conditions would explain the black colour of LF2 and similar sediment characteristics have been recognised in other epishelf lake records e.g., Disrareli Fiord (Antoniades et al., 2011) as marking a reduction of marine influence and a switch to freshwater dominance during ice shelf reformation. The suppression of biological activity expected from increasing lake ice is also supported by the presence of *Heterotrissocladius oliveri*-type chironomids, which are thought to live in the profundal zone and indicate a cold stenothermic (narrow temperature range) and possibly ultraoligotrophic environment (Winnell and White, 1986; Axford et al., 2019).

The transition from a largely marine to a fresher 'lacustrine' setting is also accompanied by a change in producers i.e., low K37/K38, increases in aquatic OM. Terrigenous inputs (terrigenous OM) increase between 274cm and 250cm, peaking during the freshest conditions at 268 cm (Fig. 8). This could relate to glacier advance, bringing with it higher concentration of detritus or detritus from different sources, as indicated by the mix of OM signatures from vegetation (CPI, Pr/Ph, C_{31}/C_{29}). The clay mineral data support variations in sediment source. Both smectite and kaolinite decrease to minima at 268.5 cm and increase thereafter. This pattern is mirrored by increases (and decreases) in illite and chlorite. This variability likely reflects a transition from a 'marine' clay mineral assemblage, whereby detritus is derived from multiple source-areas to one that is dominated by a local inputs i.e., LF3. The input of terrigenous OM and increase in aquatic OM implies enhanced lake fertilization, and we envisage that the combination of increased nutrient flux together with changes in water properties led to the change in producers at Blåsø.

LF3: This unit is a red/brown, laminated, clay/silt with occasional >2mm clasts (Fig. 4-6). Some laminae are normally graded, with distinctive clay caps. Magnetic susceptibility gradually decreases up core in LC12 (Fig. 5), while in LC7 (Fig. 4) susceptibility first increases to ~100 cm before decreasing. Minor increases in coarse-silt occur in LC12 above 60 cm (Fig. 5). Illite remains the dominant clay mineral (>50 %) but decreases relative to LF2 (Fig. 7). Smectite gradually decreases up-core from 11 % to 7%, while kaolinite increases up to 180-120 cm (~15 %) before decreasing again. Chlorite varies in the upper ~60 cm, but shows an overall increase in concentrations up core.

Foraminifera are generally absent, though rare tests occur in the upper 30 cm and in surface samples which contain calcareous and agglutinated species in very low abundances (*C. reniforme, E. excavatum, Textularia earlandii*) (Fig.4, Fig. 5). Other microfauna include chironomids, cyclorrapha (flies) and copepods, although not in datable concentrations. Ti/Ca ratios drop in this unit but exhibit distinct variability between 0-0.05 (Fig. 4, Fig. 5).

The U^K_{37} decreases throughout LF3, ranging between -0.4 and -0.7 in LF3a to between -0.6 and -0.7 in LF3b and LF3c. Conversely, $\%C_{37:4}$ increases from an average of 58% in LF3a to 66% in LF3b and LF3a. The uppermost sample, however, displays a higher U^K_{37} (-0.6) and lower $\%C_{37:4}$ (60%) values. Similar changes are observed in

the K37/K38 index, which shows lower variability (values between 1.0-1.4) compared to LF1 and LF2, with one exception at 200cm (where the index drops to 0.7), and a slow decreasing trend from an average of 1.2 in LF3a to 1.1 in LF3b and LF3c). The terrigenous and aquatic OM show a gradual increasing trend throughout LF3a with greater variability in LF3b and LF3c. The CPI first increases in LF3a from ~1 to 1.3 up to 218 cm, where it reaches a broad maximum (1-1.2) between 218 and 128cm, before decreasing through LF3b to low and stable values (0.7-0.8) in LF3c. Pristane/Phytane ratio increases from below 1 to 3.7 at 218 cm then shows an up-core decreasing trend, reaching values below 1 in LF3c. The C_{31}/C_{29} index is variable throughout LF3a (0.5-0.7) and progressively increases in LF3c and LF3c (0.6-1.0). TAR displays low values (1.1-2.7) throughout LF3a and LF3b with a shift to increasing variability and higher values (2.5-5.5) in LF3c.

Paleoenvironmental iInterpretation: The absence of foraminifera, except for rare occurrences in the upper ~30 cm, together with persistently high(low) %$C_{37:4}$(U^{K}_{37}) values implies that Blåsø remained largely isolated from marine water due to the persistence of an ice shelf. Recent analysis of Arctic surface sediments indicates that %$C_{37:4}$ concentrations between 60-70% are typically associated with ~75% sea-ice concentration (Wang et al., 2021). Thus, it seems likely that perennial lake ice existed in Blåsø which retarded, but did not completely stop, productivity in the surface water. The U^{K}_{37} values indicate warmer SWT throughout much of LF3a, with a shift to cooler conditions in LF3b-LF3c (Fig. 8). A minor increase in temperature is observed in the upper ~20 cm. The overall increase in aquatic and terrestrial OM in LF3a, indicative of higher woody vegetation (decreases in C_{31}/C_{29}), could imply a wetter climate (Bush and Mcinerney, 2013) which fertilised the surface waters in the summer melt season. An overall decrease in aquatic OM in LF3c, despite constant terrestrial OM inputs of higher grassy vegetation (increases in C_{31}/C_{29}), suggests less productivity in the lake, perhaps under drier conditions. The lower CPI and Pr/Pr ratios in LF3c likely reflects an increase in catchment erosion (Walinsky et al., 2009; Sánchez-Montes et al., 2020) although an increase in graminoids (Bush and McInerney, 2013) and more reductive conditions in the lake (Ten Haven et al., 1988) could also explain the low values. The higher TAR reflects increases in terrigenous OM and decrease in aquatic OM inputs across LF3. More generally, the laminated and graded nature of LF3 (potential varves; cf. Palmer et al. 2019) implies seasonal variations in sediment input and/or different sediment sources (fluvial/fluviodeltaic vs glacial).

As noted above, the clay mineral assemblage of LF3a-b differs markedly from that deposited in a marine setting (LF1), being characterised by >smectite, <illite, <chlorite and >kaolinite. This reflects the 'lacustrine' end-member, potentially isolated from exotic (marine) lithologies because of the ice shelf dam which would limit detritus delivered via IRD and/or sourced from a wider area. In this context, increases in smectite likely derive from the Neoproterozoic Rivieradal Group siliciclastic succession, which contains conglomerates rich in quartzite and dolerite clasts (Higgins et al., 2004), with the latter likely to be smectite-rich. The higher kaolinite could derive from shales or limestones, which are also present in the Rivieradal Group and Odins Fjord Formation respectively.

One intriguing aspect of the upper ~60 cm of LC12 (LC3c) is that it displays some of the characteristics of LF1 e.g., increases in coarse silt, chlorite and illite, Br and TAR and reduced CPI, aquatic OM, albeit with much lower numbers of foraminifera and %$C_{37:4}$ indicative of a 'fresh' water column. Indeed, a minor increase in %$C_{37:4}$ from

58 to 66% and decrease in U^K_{37} values at ~100cm imply decreasing SWT and salinities. Taken at face value this indicates that Blåsø became fresher, colder and even more isolated from marine inputs above 100 cm. However, an alternative explanation is that the minor increase in foraminifera, together with increases in clay minerals indicative of a 'marine' end-member (Fig. 7) implies incursions of marine water to the central basin. While the %$C_{37:4}$ preclude a fully mixed (marine) water column, the minor increase in foraminifera and other 'marine' markers could reflect modern ice shelf thinning or thinning in the recent past, enabling a greater proportion of marine water into the central basin. This interpretation could explain the decrease in aquatic OM despite the continuous terrigenous inputs (increase in TAR, lower CPI). However, because we have not been able to date this part of the core (LF3a-c), due to insufficient foraminifera/datable material, we cannot completely rule out that the 'marine' signature reflects re-working of uplifted glacimarine sediments within the Blåsø catchment, possibly delivered to the lake by increased catchment erosion due to climate or glacier advance and/or aeolian transport.

4.2 Uplifted glacimarine and deltaic sediments

Along the western and northern edge of Blåsø, uplifted glacimarine (BUG) and deltaic sediments occur, some of which were previously described by Bennike and Weidick (2001) (Fig. 2, 9, 10). Our field observations constrain the marine limit to ~33 m.a.s.l (Fig. 9, 10a, b), though sealake-ice push ridges were observed above this up to ~47 m.a.s.l. To the west of Blåsø the marine limit is marked by an extensive coarse gravel delta at ~ 33 m.a.s.l and this can be traced around the lake (Fig. 2). However, as relative sea-level fell through the Holocene, intermediate delta surfaces overprint the coastline at ~ 25 m and 15 m.a.s.l. We identified two main lithofacies (BUG/LF1 and BUG/LF2).

BUG/LF1: These are red/brown massive to weakly stratified clays and silts containing *in situ* macrofauna (articulated bivalves) dominated by *Hiatella arctica* (Fig. 9, Fig. 10c,d). In most exposures this lithofacies occupies an elevational range of 0-22 m.a.s.l. The predominance of silt and clay suggest this is a deeper water lithofacies which is distal to any ice-stream grounding line or local fluvial input. There are occasional dropstones indicative of ice rafted input (Fig. 10e). Benthic foraminiferal assemblages, although not assessed quantitatively, are dominated *by E. excavatum f. clavata clavatum* (Jennings et al., 2020), but also include several other glacimarine and cold water species (*C. reniforme, Islandiella islandica, Haynesina obiculare, Astononion gallowayi, Nonion spp, Triloculina tricarinata, S. feylingi, Spiroplectammina biformis, Quinqueloculina sp.* BUG/LF1 is therefore interpreted to reflect full glacimarine conditions within the basin with fine-grained nature reflecting deeper water conditions.

BUG/LF2: BUG/LF1 is overlain by planar bedded, well-sorted silty sand and fine gravels (Fig. 10f). These sediments coarsen upwards and are characterised by planar cross-bedded and trough cross-bedded structures that we interpret as incised channels. These sediments form distinctive flat-topped surfaces at varying altitudes adjacent to the lake shore. These sediments contain both reworked and *in situ* molluscan fauna dominated by *Hiatella arctica* but with minor occurrences of *Astarte borealis* and *Mya Truncata*. In several places around the lake, the upper sediment sequences are reworked into indistinct linear ridges. BUG/LF2 is interpreted as partially channelised, delta topsets which formed marginal to the lake and overlying BUG/LF1. We envisage that the delta staircase formed peripherally to the lake basin as relative sea level dropped from the marine limit at ~ 33 to ~25

475 m.a.s.l (SP2) and then to ~ 15 m.a.s.l (SP1) (Fig. 9). The distinctive ridges are most likely lake-ice push ridges (Hendy et al., 2000). S, and similar landforms were seen forming along the contemporary lake edge during fieldwork in 2017.

4.3 Chronology

480

LF1 yielded foraminiferal (mixed benthic) ages 4,170-5,670 ^{14}C yrs BP (4,042056-5,898 858 cal. yrs BP) for core LC7 and 4.345-5,910 ^{14}C yrs BP, (4.263274-6,147 127 cal. yrs BP) for core LC12 (Table 2). With the exception of one sample at 307 cm in core LC12, dated to 5,910 ^{14}C yrs BP, all ages occur in stratigraphic order within error. This age is omitted from our stratigraphy. Radiocarbon dating of the bulk organic fraction of LF1 and LF2 (LC12)

485 yielded anomalouslyanonymously old ages (11,156-22,367 ^{14}C yrs BP), which likely reflects inputs of fossil carbon from the limestone-dominated catchment. Age-depth modelling of the ^{14}C age-data (LF1) was undertaken with CLAM v2.40 using linear interpolation between neighbouring levels (Blaauw, 2010).

Shell samples (*Hiatella arctica* and gastropod) from the uplifted glacimarine and deltaic sediments yielded ages

490 of between 5,794 to 8,205 ^{14}C yrs BP (6,047022-8,519 cal. yrs BP). BUG/LF1 is dated to 7,227–7,936 cal. yrs BP. It is older than LF1 recovered from the lake cores and therefore helps to constrain the initial phase of glacimarine sedimentation in Blåsø. The sediments from BUG/LF2 record two separate phases of deltaic sedimentation peripheral to the lake. The earliest deltaic phase is recorded at site SP2 at ~ 25.11 m.a.s.l and is dated to 7,677629–8,519 cal. yrs BP (Fig. 9). This is close to the marine limit and helps to constrain both

495 deglaciation, the early formation of Blåsø and the onset of relative sea-level fall. A lower elevation deltaic site (SP1 ~ 15.93 m.a.s.l; Fig. 9) marks further sea-level fall constrained to 6,047022-6,138 114 cal. yrs BP and this is also predates the deposition of LF1 in cores LC12 and LC7.

5 Discussion

500 Analysis of two sediment cores (LC7 and LC12) recovered from the 'central basin' of Blåsø display near-identical sedimentological, faunal and geochemical/biomarker changes, thereby confirming a consistent history of deposition within the lake basin. Together with environmental and chorological information from uplifted glacimarine sediments they provide a detailed record of the Early-Mid Holocene retreat of 79°N ice shelf and its subsequent reformation. The discussion below mainly focuses on the results of LC12 since this core was analysed

505 in most detail.

5.1 Ice shelf retreat phase (~ 8.5 to 4.4 cal. ka BP):

Raised glacimarine deposits around Blåsø provide clear evidence for a complete deglaciation of the ~70km-long Nioghalvfjerdsfjorden from a more advanced Late Glacial configuration (Winkelmann et al., 2010; Rasmussen et

510 al., 2022)(Fig. 11a). The onset of deglaciation – and the earliest evidence for the absence of 79°N ice shelf – is constrained by the deposition of mollusc-bearing glacimarine sediments (BUG/LF1). These sediments formed close to the marine limit (~33 m.a.s.l) on the western side of Blåsø and have subsequently been uplifted due to

isostatic rebound (Fig. 11b). Radiocarbon dating of in-situ *Hiatella arctica* within BUG/LF1 indicate that marine conditions were established as early as ~8.5 cal. ka BP (Table 2). *Hiatella arctica* inhabits a relatively broad water depth range (0-800 m; Harbo, 1997), though the predominantly fine-grained nature of BUG/LF1 implies deposition in deeper water, distal to a grounding line. We envisage that BUG/LF1 formed as relative sea-level dropped from the marine limit at ~33 m.a.s.l to ~15 m.a.s.l (Fig. 11b). While the timing of sea-level drop is poorly constrained by our data, radiocarbon dating of gastropods within uppermost delta topsets records postglacial sea-level fall until ~ 6.0 cal. ka BP. The evidence for ice shelf absence between 8.5 and 4.0 cal. ka BP is consistent with previously published ^{14}C dates from molluscs and whale bones which indicated that the ice shelf was smaller than present ~7.8-4.6 cal. ka. BP (Bennike and Weidick, 2001). The ages presented here extend the ice free period by over a millennium. The chronology is also consistent with [10]Be ages which indicate the deglaciation of Nioghalvfjerdsfjorden occurred between 9.2 and 7.9 ka (Larsen et al., 2018).

The lowermost sediments in LC12 and ~~LF7~~ LC7 (LF1) are characterized by an exclusively open marine micro-fossil assemblage and alkenone profiles consistent with fully-mixed (saline) water column. This confirms that the ice shelf retreated and also adds additional insights into the environmental conditions close to the grounding line of 79°N Glacier. [14]C data from LC7 and LC12 indicates that the Blåsø catchment was inundated by marine waters between 5.9 and 4.0 cal. ka BP (Table 2). The foraminiferal fauna in both cores is characteristic of relatively 'cold' Arctic water conditions, likely influenced by the input of glacial meltwater from nearby tidewater glacial margins as 79°N Glacier re-advanced and the ice shelf started to reform (Fig. 11c).

Multiple lines of evidence indicates that retreat of 79°N ice shelf occurred at a time of atmospheric and ocean warming (Fig. 12). A compilation of ice core records and model simulations indicate the most pronounced summer warming occurred from ~10 to 6 ka i.e., HTM, roughly in phase, but lagging maximum summer insolation (Buizert et al., 2018). Maximum atmospheric warmth across Greenland is supported by a chironomid-based temperature maxima ~8–5 cal. ka BP from a lake on nearby Store Koldeway (Klug et al., 2009). Similarly, marine records from the eastern Fram Strait, as well as directly in front of 79°N ice shelf, reveal a consistent picture of warm sea surface, subsurface and bottom water temperatures during the HTM. Foraminifera-based transfer functions indicate sea-surface to sub-surface temperatures of up to 6°C until ~5 cal. ka BP, in the Fram Strait, with maximum seawater temperatures occurring ~10 to 8 cal. ka BP (Fig. 12) (Werner et al., 2016). Assemblage data from the same core also indicate ~~persistent~~ Atlantic Water persisted in Fram Strait ~~advection~~ between 10.6 and 8.5 cal. ka BP, related to maximum July insolation (Werner et al., 2016). Multi-proxy data from core PS100/270, 16-km from the calving front of 79°N ice shelf (Fig. 11), indicates strong inflow of warm recirculating Atlantic Water between ~10 and 7.5 cal. ka BP (Syring et al., 2020) and this is consistent with foraminifera assemblage data from a core in inner Norsk Trough, which indicate a shift towards warmer conditions, increase in nutrient supply and higher productivity between 9.6–7.9 cal. ka BP (Davies et al., 2022). The relative abundance of the Atlantic Indicator *C. neoteretis* remains relatively high until approx. 6.5 cal. ka BP in core PS100/270, but then decreases as the relatively cold-water indicator, *C. reniforme*, increases to over 40% of the assemblage after ~6.0 cal. ka BP (Syring et al., 2020).

Comparable environmental changes are also recorded in cores from the mid-shelf where cold, sea ice-covered surface waters and a strong subsurface influx of warm Atlantic water has been documented ~9.4 and 8.2 cal. ka B.P (Pados-Dibattista et al., 2022). The authors also note a peak in IRD at ~8.4 cal. ka BP, which they attribute the influx of terrestrially derived detritus associated with break-up of 79°N ice shelf. These data are consistent with our observations of open marine conditions in Blåsø by 8.5 cal. ka BP and when viewed together with other proxy data, confirm that 79°N had retreated inboard of its present location after almost two millennium of elevated atmospheric and ocean temperatures.

While the exact retreat configuration of 79°N Glacier and ice shelf is unclear from our data, we suspect that grounding line retreat of the glacier was accompanied by ice shelf thinning, driven from above and below, leading to eventual loss of the ice shelf in the Early Holocene and the formation of a tidewater calving margin, similar to the fate of Zachariae Isstrøm post 2010 (Khan et al., 2014; Mouginot et al., 2015; An et al., 2021). Complete disintegration of the ice shelf is supported by the presence of driftwood, whale and seal bones along Nioghalvfjerdsfjorden and around the shore of Blasø, dated to 7.7 and 4.5 cal. ka BP (Bennike and Weidick, 2001). This trajectory of Early Holocene ice shelf loss thus seems similar to the present-day, with enhanced basal and surface melting leading to ice shelf thinning and grounding line retreat. It is also possible that after several centuries where mean-annual temperatures exceeded current levels, extensive melt-pools formed on the ice shelf surface (e.g., Turton et al., 2021), which eventually resulted in hydrofracture and catastrophic collapse of the ice shelf. Indeed, the glacial reconstruction of Syring et al. (2020) indicates retreat of an expanded 79°N ice shelf to a position similar to present after 9.6 cal. ka BP meaning that the ice shelf must have lost its entire area between ~9.6 and 8.5 cal. ka BP. It is likely that collapse of the ice shelf during the Early-Mid Holocene was accompanied by retreat of 79°N Glacier, although the inland extent of this in unconstrained by our data and should be explored with an ice sheet model.

5.2 Ice shelf re-formation phase and re-establishment of the epishelf lake at Blåsø (~ 4.4 to 4.0 cal. ka BP):

Our multi-proxy data set indicate a clear shift from an open (glaci)marine setting to one characterised by the increasing isolation of Blåsø from the marine water circulating in Nioghalvfjerdsfjorden. This started as a build-up of sea/lake ice after ~4.4 cal. ka BP, with increasing numbers of *S. horvathi,* culminating in complete isolation of Blåsø by 4.0 cal. ka BP as the ice shelf thickened and re-grounded at the western and eastern ends of Blåsø (Fig. 11c). The combination of thick sea-ice and closure of Blåsø after ~4.0 cal. ka. BP, acted to limit photosynthesis and exchange with the atmosphere and ocean, and over the course of decades, resulted in oxygen depletion and a period of anoxic conditions in the lake and lower aquatic productivity (Fig. 11d). Based on interpolation of ^{14}C ages, the anoxic event lasted ~500 years i.e., until 3.5 cal. ka. BP, although this is highly uncertain.

Grounding line advance is assumed to be accompanied by reformation of the ice shelf, and this occurred at a time when proxy records indicate climate cooling (Fig. 12). In the Fram Strait, a weakened Atlantic Water contribution occurs after ~5.0 cal. ka BP, when subsurface temperatures decrease rapidly with minimum values observed between ~4.0 and 3.0 cal. ka BP (Werner et al., 2016). On the continental shelf, Syring et al. (2020) document

near perennial sea-ice conditions with only short summers from ~7.5 to ~0.8 cal. ka BP directly adjacent to 79°N ice shelf while Pados-Dibattista et al. (2022) have suggested (near) perennial sea-ice cover after ~4.2 cal. ka BP, associated with increased Polar Water at the surface of the East Greenland Current, and a reduction in the Return

595   Atlantic Water at subsurface levels. Both ice core and chironomid-inferred records of atmospheric temperature indicate that ocean cooling was accompanied by decreasing air temperatures (Buizert et al., 2018; Klug et al., 2009). Summer (June-July-August) temperatures at 79°N fall steadily from ~7.9 cal. ka BP, reaching ~2.0°C by 4.5 cal. ka BP (Fig. 12) (Buizert et al., 2018). Similarly, the chironomids *Procladius* and *C. oliveri*-type decline in abundance in Duck Lake (Store Koldeway; Fig. 1a), which is likely to be related to deteriorating living

600   conditions associated with the long-term decrease in summer air temperatures (Klug et al., 2009). In the absence of warm Atlantic Water circulating in the fiord and declining air temperatures, it is likely that the grounding line advanced and the ice shelf reformed, probably as a composite ice shelf. Build-up of sea-ice, potentially from as early as ~7.5 cal. ka BP (Syring et al., 2020), would have combined with increased snow accumulation (Rasmussen et al., 2013) to thicken and form multi-year sea/fast-ice. This would have buttressed the ice shelf

605   allowing it to thicken and advance in tandem with the grounding line (Higgins, 1991; Robel, 2017). After ~4.4 cal. ka BP, the ice shelf had thickened and advanced sufficiently to begin impeding the circulation of marine waters in Blåsø, initiating formation of the epishelf lake. The up-fiord advance of the ice shelf is poorly constrained by our data but the absence of ages younger than ~4.5 cal. ka BP at 'Midgårdsormen base camp' (Fig. 1) (Bennike and Weidick, 2001) suggests the ice shelf had advanced to at least this position. Given that the

610   Midgårdsormen base camp is ~15 km east of Blåsø's eastern mouth, the concurrent grounding of the ice shelf at both sites indicates that the ice shelf had started to re-form and advance across the fiord well before ~4.5 cal. ka BP.

5.3 Epishelf lake phase (~4.0 cal. ka. BP, to present):

615   An epishelf lake was established by ~4.0 cal. ka BP, following continued (Neoglacial) cooling (Fig. 11e). There is no indication for a ~~switch back~~return to marine-dominated conditions in Blåsø since then, suggesting that 79°N Glacier remained grounded at the western mouth~~s~~ of the lake and the rest of the fiord was continuously covered by an ice shelf from the Mid/Late Holocene to present-day. Throughout this period, Blåsø was likely covered by perennial lake ice, which appears to have been more dominant for the latter part of the record (upper 100 cm in

620   LC12, LF3b and LF3c (Fig. 5)). Although uncertain, linear interpolation of the ^{14}C data indicates that LF3b and LF3c span~~s~~ the past ~2 ka. Despite the lack of robust dating control, our multi-proxy data indicate~~s~~ variable sediment input into the lake, likely associated with catchment dynamics driven by climate variability. Wetter catchment conditions are inferred for LF3a/b (increases in aquatic and terrestrial and of higher woody vegetation (decreases in C31/C29; Meyer, 2003), while an overall decrease in aquatic OM and increases in C31/C39 in LF3c

625   (uppermost ~60 cm), suggest less productivity in the lake, possibly during a drier climate. In the nearby Trifna Sø catchment (Fig. 1a), 50 km north of Blåsø, soil erosion peaked around c. 3.4 to 3.0 cal. ka BP, and the vegetation assemblage became more variable thereafter (Kusch et al., 2019). To the south, Duck Lake on Store Koldeway records a prolonged phase of lake ice cover from 2.0 cal. ka BP (Klug et al., 2009). In addition, high TIC values in Duck Lake between 1.3 and 0.8 cal. ka BP, punctuated by a decrease at 1.0 cal. ka BP, have been interpreted

630   to represent phases of high productivity during periods of warmer summers. A similar pattern of high-productivity separated by a drop in productivity has also been observed in other lakes records from East and Northeast

Greenland (Wagner and Melles, 2001; Wagner et al., 2000). On the adjacent mid-shelf, foraminiferal data imply cold and unstable oceanic conditions, with minimum surface-water productivity and possibly sea-ice cover from ~3.2 until 0.3 cal. ka BP (Pados-Dibattista et al., 2022). The latter study attributes this to a strengthened East Greenland Current resulting in a thick, cold and fresh layer of Polar Water on the surface and strong recirculated Arctic Atlantic Water inflow at subsurface levels. Syring et al. (2020) point to a minimum solar insolation during the middle to late Holocene to explain the strengthened East Greenland Current and the influence of colder polar waters toward the inner shelf. It seems likely that some of the changes observed in Blåsø, relate to regional climate variability, likely driven by changes in atmospheric moisture content. While additional dating constraints are required in order to enable comparisons with other records, we suggest that generally wetter conditions persisted from ~4 cal. ka BP to around ~2 cal. ka BP, with more variability and possibly a move to drier conditions recorded thereafter.

A final possibility – and one discussed above – is that the variability in proxies in the uppermost ~60-50 cm of LC12 relates to recent (past ~100 years) thinning of 79°N allowing greater ingress of marine water (Fig. 11f). However, while the clay mineral assemblage shares similar attributes to the marine facies (LF1) and the presence of small numbers of calcareous micro-fossils could suggest renewed influence of marine water, the %$C_{37:4}$ ratio do not support increased salinity in the central basin. In this context, Bennike and Weidick (2001) have suggested that the 79°N ice shelf reached its maximum extent during the Little Ice Age (LIA) in response to Neoglacial cooling. Thus, it is possible that some of the changes we see in the upper ~60 cm might relate to a reconfiguration of the ice shelf following LIA advance. In theory this could introduce re-worked uplifted glacimarine sediments containing (early/mid Holocene-age) foraminifera and a distinctive clay mineral signature. However, further work is required to decipher the significance of these changes with particular focus on dating the uppermost part of LC12.

5.4 Sensitivity of 79°N ice shelf to post-LIA warming

Over the past decade, thinning and retreat of the floating portion of 79°N Glacier has raised concerns that its collapse is an inevitable consequence of continued climate warming. We show that past retreat of 79°N Glacier and collapse of its floating tongue occurred during the HTM, when atmospheric and ocean temperatures were similar to today or, within the projected scenarios (CMIP6) for the middle or end of this century (Hofer et al., 2020) (Fig. 12). Specifically, the data-model reconstruction of Buizert et al. (2018) suggest that the HTM summer temperatures were ~3.3°C above modern, although mean annual temperatures were closer to ~2.0°C above modern. While there is a lack of comparable ocean data, particularly proximal to 79°N, proxy-based reconstructions from the Fram Strait indicate that ocean temperatures during the HTM were ~2°C warmer than historical data (1955-2012) (Werner et al., 2016). Currently, warm Atlantic Water from the Fram Strait is driven toward the glaciers in northeast Greenland via Ekman pumping over the shelf-break (Munchow et al., 2020) and it seems reasonable to assume similar processes operated in the past. In addition to being warmer, 'peak' ocean and atmospheric temperatures during the HTM persisted for at least 1.7 and 1.4 ka respectively, prior to the retreat of 79°N ice shelf inboard of Blåsø (Fig. 12). The corollary of this is that the ice shelf was resilient under centuries to millennia of thermal forcing. However, it is worth noting that the HTM occurred while the ice sheet was

retreating from a more advanced state, meaning that it was likely thicker and potentially more resilient to this past warm interval. Given the demise of neighbouring Zachariæ Isstrøm in 2015 (Mouginot et al., 2015) under intensified thermal forcing, and the more recent collapse of Spalte Glacier in 2020, it seems reasonable to assume that 79°N ice shelf will suffer the same fate. Taking the HTM ocean and atmosphere temperatures as a threshold for the loss of 79°N ice shelf (acknowledging that this is likely an upper limit for this scenario), the ~2.0°C warming of the atmosphere may occur as early as 2060 (under high emissions scenarios RCP8.5) (Fig. 12) (Hofer et al., 2020), while ocean temperatures are also expected to reach 2.0°C warmer than present by the end of the century (Yin et al., 2011). In this context there is an urgent requirement for numerical modelling, utilising the timing of changes presented in this study together with information on ocean and atmospheric forcing, to investigate the response of NEGIS to retreat or loss of the ice shelf. Previous modelling work with fixed, present-day (atmospheric) seasonality, could not produce a clear HTM minimum in ice sheet extent (Lecavalier et al., 2014; Buizert et al., 2018). The inability of the latter models to drive significant GrIS retreat likely relates to the lack of ocean forcing (Buizert et al., 2018). Indeed, most ice sheet numerical models used to project sea level rise from the GrIS do not include realistic ocean thermal forcing (Goelzer et al., 2020) and this needs to be included in future model simulations.

6 Conclusions

- High-resolution, multi-proxy sediment records from an epishelf lake in northeast Greenland, together with dates on marine molluscs in uplifted glacimarine sediments show that the 79°N ice shelf was ~70 km inboard of the present ice shelf margin during the Early to Mid-Holocene between ~8.5 and 4.4 cal. ka BP. Ice shelf collapse was also likely to be accompanied by retreat of 79°N Glacier, although the inland extent of this in unconstrained by our data.

- The timing of ice shelf retreat through Nioghalvfjerdsfjorden followed a period of thermal forcing when atmospheric and ocean temperatures were >2°C warmer than present and were sustained for at least a millennia prior to ice shelf collapse/retreat. While this implies some resilience to thermal forcing, the ice sheet/shelf was retreating from an advanced position following the Last Glacial Maximum, meaning that it was likely thicker and potentially more resistant to climate change during the Early Holocene.

- The ice shelf reformed from ~4.4 to 4.0 cal. ka BP during a phase of climatic cooling although the precise spatial pattern of reformation is not known. We speculate that the ice shelf reformed via thickening of sea-ice, which helped buttress and thicken an advancing ice tongue.

- Our reconstruction suggests that 79°N ice shelf is vulnerable to collapse when atmospheric and ocean temperatures are >2°C warmer than present, which could be achieved by the middle of this century under some climate model scenarios.

- Finally, the uppermost ~60 cm of the epishelf lake core record, displays characteristics similar to that observed during the Early Holocene collapse. This could suggest that recent thinning of 79°N ice shelf is now detected in Blåsø although further work – particularly focussing on generating new age-constraints – are required to test this hypothesis.

Data availability

The datasets used in this paper are available at the NERC Polar Data Centre (http://www.bas.ac.uk/data/uk-pdc/).

Competing interests

The authors declare that they have no conflict of interest.

Author contribution

JAS, MJB, DRH, SJ, JML, BRR and CO conceived the study and JAS wrote the initial draft. JAS, MJB, SJ, TL recovered the lakes sediment cores and DHR, JAS, MJB, TL and CD sampled the uplifted glacimarine sediments. LC split, described, sampled and performed non-destructive analyses (physical properties, XRF scanning) of the lake core, with help from DHR and JAS. JML undertook the foraminiferal work, MLS performed the biomarker analyses with ELM, WE analysed the clay minerals, and ~~SM~~ PG performed the ^{14}C dating at SUERC. All authors discussed the results and implications and collaborated on writing the manuscript.

Acknowledgements

This work was funded by NERC Standard Grant NE/N011228/1 and some radiocarbon analysis funded by NEIF under grant NE/S011587/1 (allocation number 2169.1118)~~This work was funded by NERC Standard Grant NE/N011228/1 and NEIF radiocarbon allocation number 2169.1118~~. We thank the Alfred Wegner Institute, and particularly Angelika Humbert and Hicham Rafiq, for their significant logistic support through the iGRIFF project. Additional support was provided from Station Nord (Jorgen Skafte), Nordland Air, Air Greenland and the Joint Arctic Command. Naalakkersuisut, Government of Greenland, provided Scientific Survey (VU-00121) and Export (046/2017) licences for this work. Finally, we would like to thank our Field Ranger Isak (Nanu-Travel) and dog Ooni for keeping us safe in the field and taking great pleasure in beating JAS at cards.

References

730   An, L., Rignot, E., Wood, M., Willis, J. K., Mouginot, J., and Khan, S. A.: Ocean melting of the Zachariae Isstrom and Nioghalvfjerdsfjorden glaciers, northeast Greenland, Proc. Natl. Acad. Sci. U. S. A., 118, 10.1073/pnas.2015483118, 2021.

Antoniades, D., Francus, P., Pienitz, R., St-Onge, G., and Vincent, W. F.: Holocene dynamics of the Arctic's largest ice shelf, Proc. Natl. Acad. Sci. U. S. A., 108, 18899-18904, 10.1073/pnas.1106378108, 735   2011.

Arz, H., Patzold, J., and Wefer, G.: Climatic changes during the last deglaciation recorded in sediment cores from the northeastern Brazilian Continental Margin, Geo-Marine Letters 19, 209-218, 1999.

Aschwanden, A., Fahnestock, M. A., Truffer, M., Brinkerhoff, D. J., Hock, R., Khroulev, C., Mottram, R., and Khan, S. A.: Contribution of the Greenland Ice Sheet to sea level over the next millennium, 740   Science Advances, 5, 10.1126/sciadv.aav9396, 2019.

Axford, Y., Lasher, G. E., Kelly, M. A., Osterberg, E. C., Landis, J., Schellinger, G. C., Pfeiffer, A., Thompson, E., and Francis, D. R.: Holocene temperature history of northwest Greenland - With new ice cap constraints and chironomid assemblages from Deltaso, Quat. Sci. Rev., 215, 160-172, 10.1016/j.quascirev.2019.05.011, 2019.

745   Bahr, A., Lamy, F., Arz, H., Kuhlmann, H., and Wefer, G.: Late glacial to Holocene climate and sedimentation history in the NW Black Sea, Mar. Geol., 214, 309-322, 10.1016/j.margeo.2004.11.013, 2005.

Bendle, J. and Rosell-Mele, A.: Distributions of U-37(K) and U-37 '(K) in the surface waters and sediments of the Nordic Seas: Implications for paleoceanography, Geochem. Geophys. Geosyst., 5, 750   10.1029/2004gc000741, 2004.

Bennike, O. and Weidick, A.: Late Quaternary history around Nioghalvfjerdsfjorden and Jokelbugten, North-East Greenland, Boreas, 30, 205-227, 10.1080/030094801750424139, 2001.

Bentley, M. J., Hodgson, D. A., Sugden, D. E., Roberts, S. J., Smith, J. A., Leng, M. J., and Bryant, C.: Early Holocene retreat of the George VI Ice Shelf, Antarctic Peninsula, Geology, 33, 173-176, 755   10.1130/g21203.1, 2005.

Bentley, M. J., Smith, J. A., Jamieson, S. S. R., Lindeman, M. R., Rea, B. R., Roberts, D. H., Lane, T., Darvill, C. M., Lloyd, J. M., Straneo, F., and Humbert, A.: Direct measurement of warm Atlantic Intermediate Water close to the grounding line of Nioghalvfjerdsfjorden (79N) Glacier, North-east Greenland, The Cryosphere Discussions, https://doi.org/10.5194/tc-2022-206, 2022.

760   Blaauw, M.: Methods and code for 'classical' age-modelling of radiocarbon sequences, Quaternary
       Geochronology, 5, 512-518, 10.1016/j.quageo.2010.01.002, 2010.

       Blau, M. T., Turton, J. V., Sauter, T., and Molg, T.: Surface mass balance and energy balance of the
       79N Glacier (Nioghalvfjerdsfjorden, NE Greenland) modeled by linking COSIPY and Polar WRF,
       Journal of Glaciology, 67, 1093-1107, 10.1017/jog.2021.56, 2021.

765   Bray, E. E. and Evans, E. D.: Distribution of n-paraffins as a clue to recognition of source beds,
       Geochim. Cosmochim. Acta, 22, 2-15, https://doi.org/10.1016/0016-7037(61)90069-2, 1961.

       Buizert, C., Keisling, B. A., Box, J. E., He, F., Carlson, A. E., Sinclair, G., and DeConto, R. M.:
       Greenland-Wide Seasonal Temperatures During the Last Deglaciation, Geophys. Res. Lett., 45, 1905-
       1914, 10.1002/2017GL075601, 2018.

770   Bush, R. T. and McInerney, F. A.: Leaf wax n-alkane distributions in and across modern plants:
       Implications for paleoecology and chemotaxonomy, Geochim. Cosmochim. Acta, 117, 161-179,
       10.1016/j.gca.2013.04.016, 2013.

       Cage, A. G., Pienkowski, A. J., Jennings, A., Knudsen, K. L., and Seidenkrantz, M. S.: Comparative
       analysis of six common foraminiferal species of the genera Cassidulina, Paracassidulina, and Islandiella
775   from the Arctic-North Atlantic domain, Journal of Micropalaeontology, 40, 37-60, 10.5194/jm-40-37-
       2021, 2021.

       Choi, Y., Morlighem, M., Rignot, E., Mouginot, J., and Wood, M.: Modeling the Response of
       Nioghalvfjerdsfjorden and Zachariae Isstrom Glaciers, Greenland, to Ocean Forcing Over the Next
       Century, Geophys. Res. Lett., 44, 11071-11079, 10.1002/2017gl075174, 2017.

780   Consolaro, C., Rasmussen, T. L., and Panieri, G.: Palaeoceanographic and environmental changes in
       the eastern Fram Strait during the last 14,000 years based on benthic and planktonic foraminifera, Mar.
       Micropaleontol., 139, 84-101, 10.1016/j.marmicro.2017.11.001, 2018.

       Cranwell, P. A.: Branched-chain and cyclopropanoid acids in a recent sediment, Chem. Geol., 11, 307-
       313, 10.1016/0009-2541(73)90101-0, 1973.

785   D'Andrea, W. J., Huang, Y. S., Fritz, S. C., and Anderson, N. J.: Abrupt Holocene climate change as an
       important factor for human migration in West Greenland, Proc. Natl. Acad. Sci. U. S. A., 108, 9765-
       9769, 10.1073/pnas.1101708108, 2011.

       Davies, J., Mathiasen, A. M., Kristiansen, K., Hansen, K. E., Wacker, L., Alstrup, A. K. O., Munk, O.
       L., Pearce, C., and Seidenkrantz, M.-S.: Linkages between ocean circulation and the Northeast

790   Greenland Ice Stream in the Early Holocene, Quat. Sci. Rev., 286, 107530, https://doi.org/10.1016/j.quascirev.2022.107530, 2022.

Ehrmann, W., Hillenbrand, C.-D., Smith, J. A., Graham, A. G. C., Kuhn, G., and Larter, R. D.: Provenance changes between recent and glacial-time sediments in the Amundsen Sea embayment, West Antarctica: clay mineral assemblage evidence, Antarct. Sci., 23, 471-486,
795   10.1017/s0954102011000320, 2011.

Evans, D. and Benn, D. I.: A Practical Guide to the Study of Glacial Sediments, Edward Arnold, London2004.

Fettweis, X., Box, J. E., Agosta, C., Amory, C., Kittel, C., Lang, C., van As, D., Machguth, H., and Gallee, H.: Reconstructions of the 1900-2015 Greenland ice sheet surface mass balance using the
800   regional climate MAR model, Cryosphere, 11, 1015-1033, 10.5194/tc-11-1015-2017, 2017.

Funder, S.: 14C-dating of samples collected during the 1979 expedition to North Greenland, The Geological Survey of Greenland Report 110, 9-13, 1982.

Goelzer, H., Nowicki, S., Payne, A., Larour, E., Seroussi, H., Lipscomb, W. H., Gregory, J., Abe-Ouchi, A., Shepherd, A., Simon, E., Agosta, C., Alexander, P., Aschwanden, A., Barthel, A., Calov, R.,
805   Chambers, C., Choi, Y., Cuzzone, J., Dumas, C., Edwards, T., Felikson, D., Fettweis, X., Golledge, N. R., Greve, R., Humbert, A., Huybrechts, P., Le Clec'h, S., Lee, V., Leguy, G., Little, C., Lowry, D. P., Morlighem, M., Nias, I., Quiquet, A., Ruckamp, M., Schlegel, N. J., Slater, D. A., Smith, R. S., Straneo, F., Tarasov, L., van de Wal, R., and van den Broeke, M.: The future sea-level contribution of the Greenland ice sheet: a multi-model ensemble study of ISMIP6, Cryosphere, 14, 3071-3096, 10.5194/tc-
810   14-3071-2020, 2020.

Guillemot, T., Bichet, V., Gauthier, E., Zocatelli, R., Massa, C., and Richard, H.: Environmental responses of past and recent agropastoral activities on south Greenlandic ecosystems through molecular biomarkers, Holocene, 27, 783-795, 10.1177/0959683616675811, 2017.

Hald, M. and Korsun, S.: Distribution of modern benthic foraminifera from fjords of Svalbard,
815   European Arctic, Journal of Foraminiferal Research, 27, 101-122, 10.2113/gsjfr.27.2.101, 1997.

Hanna, E., Cappelen, J., Fettweis, X., Mernild, S. H., Mote, T. L., Mottram, R., Steffen, K., Ballinger, T. J., and Hall, R.: Greenland surface air temperature changes from 1981 to 2019 and implications for ice-sheet melt and mass-balance change, Int. J. Climatol., 41, E1336-E1352, 10.1002/joc.6771, 2021.

Hansen, K. E., Lorenzen, J., Davies, J., Wacker, L., Pearce, C., and Seidenkrantz, M.-S.: Deglacial to
820 Mid Holocene environmental conditions on the northeastern Greenland shelf, western Fram Strait,
Quat. Sci. Rev., 293, 107704, https://doi.org/10.1016/j.quascirev.2022.107704, 2022.

Heaton, T. J., Bard, E., Bronk Ramsey, C., Butzin, M., Hatté, C., Hughen, K. A., Köhler, P., and Reimer,
P. J.: A RESPONSE TO COMMUNITY QUESTIONS ON THE MARINE20 RADIOCARBON AGE
CALIBRATION CURVE: MARINE RESERVOIR AGES AND THE CALIBRATION OF 14C
825 SAMPLES FROM THE OCEANS, Radiocarbon, 1-27, 10.1017/RDC.2022.66, 2022.

Heaton, T. J., Köhler, P., Butzin, M., Bard, E., Reimer, R. W., Austin, W. E. N., Bronk Ramsey, C.,
Grootes, P. M., Hughen, K. A., Kromer, B., Reimer, P. J., Adkins, J., Burke, A., Cook, M. S., Olsen, J.,
and Skinner, L. C.: Marine20—The Marine Radiocarbon Age Calibration Curve (0–55,000 cal BP),
Radiocarbon, 62, 779-820, 10.1017/RDC.2020.68, 2020.

830 Hendy, C. H., Sadler, A. J., Denton, G. H., and Hall, B. L.: Proglacial lake-ice conveyors: A new
mechanism for deposition of drift in polar environments, Geogr. Ann. Ser. A-Phys. Geogr., 82A, 249-
270, 2000.

Higgins, A. and Kalsbeek, F.: East Greenland Caledonides: stratigraphy, structure and geochronology,
Geological Survey of Denmark and Greenland Bulletin, 06, 10.34194/geusb.v6.4814, 2004.

835 Higgins, A. K.: North Greenland glacier velocities and calf ice production, Polarforschung, 60, 1-23,
1991.

Higgins, A. K., Soper, N. J., Smith, M. P., and Rasmussen, J. A.: The Caledonian thin-skinned thrust
belt of Kronprins Christian Land, eastern North Greenland, GEUS Bulletin, 6, 41-56,
10.34194/geusb.v6.4817, 2004.

840 Hochreuther, P., Neckel, N., Reimann, N., Humbert, A., and Braun, M.: Fully Automated Detection of
Supraglacial Lake Area for Northeast Greenland Using Sentinel-2 Time-Series, Remote Sensing, 13,
10.3390/rs13020205, 2021.

Hofer, S., Lang, C., Amory, C., Kittel, C., Delhasse, A., Tedstone, A., and Fettweis, X.: Greater
Greenland Ice Sheet contribution to global sea level rise in CMIP6, Nature Communications, 11,
845 10.1038/s41467-020-20011-8, 2020.

Jennings, A., Andrews, J., and Wilson, L.: Holocene environmental evolution of the SE Greenland Shelf
North and South of the Denmark Strait: Irminger and East Greenland current interactions, Quat. Sci.
Rev., 30, 980-998, 10.1016/j.quascirev.2011.01.016, 2011.

Jennings, A., Andrews, J., Reilly, B., Walczak, M., Jakobsson, M., Mix, A., Stoner, J., Nicholls, K. W., and Cheseby, M.: Modern foraminiferal assemblages in northern Nares Strait, Petermann Fjord, and beneath Petermann ice tongue, NW Greenland, Arct. Antarct. Alp. Res., 52, 491-511, 10.1080/15230430.2020.1806986, 2020.

Jennings, A. E., Weiner, N. J., Helgadottir, G., and Andrews, J. T.: Modern foraminiferal faunas of the southwestern to northern Iceland shelf: Oceanographic and environmental controls, Journal of Foraminiferal Research, 34, 180-207, 10.2113/34.3.180, 2004.

Joughin, I., Smith, B. E., Howat, I. M., Scambos, T., and Moon, T.: Greenland flow variability from ice-sheet-wide velocity mapping, Journal of Glaciology, 56, 415-430, 10.3189/002214310792447734, 2010.

Khan, S. A., Kjaer, K. H., Bevis, M., Bamber, J. L., Wahr, J., Kjeldsen, K. K., Bjork, A. A., Korsgaard, N. J., Stearns, L. A., van den Broeke, M. R., Liu, L., Larsen, N. K., and Muresan, I. S.: Sustained mass loss of the northeast Greenland ice sheet triggered by regional warming, Nature Climate Change, 4, 292-299, 10.1038/nclimate2161, 2014.

Klug, M., Schmidt, S., Bennike, O., Heiri, O., Melles, M., and Wagner, B.: Lake sediments from Store Koldewey, Northeast Greenland, as archive of Late Pleistocene and Holocene climatic and environmental changes, Boreas, 38, 59-71, 10.1111/j.1502-3885.2008.00038.x, 2009.

Kornilova, O. and Rosell-Mele, A.: Application of microwave-assisted extraction to the analysis of biomarker climate proxies in marine sediments, Org. Geochem., 34, 1517-1523, 10.1016/s0146-6380(03)00155-4, 2003.

Kusch, S., Bennike, O., Wagner, B., Lenz, M., Steffen, I., and Rethemeyer, J.: Holocene environmental history in high-Arctic North Greenland revealed by a combined biomarker and macrofossil approach, Boreas, 48, 273-286, 10.1111/bor.12377, 2019.

Larsen, N. K., Levy, L. B., Carlson, A. E., Buizert, C., Olsen, J., Strunk, A., Bjork, A. A., and Skov, D. S.: Instability of the Northeast Greenland Ice Stream over the last 45,000 years, Nature Communications, 9, 10.1038/s41467-018-04312-7, 2018.

Lecavalier, B. S., Milne, G. A., Simpson, M. J. R., Wake, L., Huybrechts, P., Tarasov, L., Kjeldsen, K. K., Funder, S., Long, A. J., Woodroffe, S., Dyke, A. S., and Larsen, N. K.: A model of Greenland ice sheet deglaciation constrained by observations of relative sea level and ice extent, Quat. Sci. Rev., 102, 54-84, 10.1016/j.quascirev.2014.07.018, 2014.

Leeson, A. A., Shepherd, A., Briggs, K., Howat, I., Fettweis, X., Morlighem, M., and Rignot, E.:
Supraglacial lakes on the Greenland ice sheet advance inland under warming climate, Nature Climate
Change, 5, 51-55, 10.1038/nclimate2463, 2015.

Mayer, C., Schaffer, J., Hattermann, T., Floricioiu, D., Krieger, L., Dodd, P. A., Kanzow, T., Licciulli,
C., and Schannwell, C.: Large ice loss variability at Nioghalvfjerdsfjorden Glacier, Northeast-
Greenland, Nature Communications, 9, 2768, 10.1038/s41467-018-05180-x, 2018.

McClymont, E. L., Rosell-Mele, A., Giraudeau, J., Pierre, C., and Lloyd, J. M.: Alkenone and coccolith
records of the mid-Pleistocene in the south-east Atlantic: Implications for the U(37)(K) index and South
African climate, Quat. Sci. Rev., 24, 1559-1572, 10.1016/j.quascirev.2004.06.024, 2005.

Morlighem, M., Williams, C. N., Rignot, E., An, L., Arndt, J. E., Bamber, J. L., Catania, G., Chauche,
N., Dowdeswell, J. A., Dorschel, B., Fenty, I., Hogan, K., Howat, I., Hubbard, A., Jakobsson, M.,
Jordan, T. M., Kjeldsen, K. K., Millan, R., Mayer, L., Mouginot, J., Noel, B. P. Y., O'Cofaigh, C.,
Palmer, S., Rysgaard, S., Seroussi, H., Siegert, M. J., Slabon, P., Straneo, F., van den Broeke, M. R.,
Weinrebe, W., Wood, M., and Zinglersen, K. B.: BedMachine v3: Complete Bed Topography and
Ocean Bathymetry Mapping of Greenland From Multibeam Echo Sounding Combined With Mass
Conservation, Geophys. Res. Lett., 44, 11051-11061, 10.1002/2017gl074954, 2017.

Mottram, R., B. Simonsen, S., Høyer Svendsen, S., Barletta, V. R., Sandberg Sørensen, L., Nagler, T.,
Wuite, J., Groh, A., Horwath, M., Rosier, J., Solgaard, A., Hvidberg, C. S., and Forsberg, R.: An
Integrated View of Greenland Ice Sheet Mass Changes Based on Models and Satellite Observations,
Remote Sensing, 11, 1407, 2019.

Mouginot, J., Rignot, E., Scheuchl, B., Fenty, I., Khazendar, A., Morlighem, M., Buzzi, A., and Paden,
J.: Fast retreat of Zachariæ Isstrøm, northeast Greenland, Science, 350, 1357-1361,
doi:10.1126/science.aac7111, 2015.

Munchow, A., Schaffer, J., and Kanzow, T.: Ocean Circulation Connecting Fram Strait to Glaciers off
Northeast Greenland: Mean Flows, Topographic Rossby Waves, and Their Forcing, J. Phys. Oceanogr.,
50, 509-530, 10.1175/jpo-d-19-0085.1, 2020.

Nace, T. E., Baker, P. A., Dwyer, G. S., Silva, C. G., Rigsby, C. A., Burns, S. J., Giosan, L., Otto-
Bliesner, B., Liu, Z. Y., and Zhu, J.: The role of North Brazil Current transport in the paleoclimate of
the Brazilian Nordeste margin and paleoceanography of the western tropical Atlantic during the late
Quaternary, Paleogeogr. Paleoclimatol. Paleoecol., 415, 3-13, 10.1016/j.palaeo.2014.05.030, 2014.

Naeher, S., Gilli, A., North, R. P., Hamann, Y., and Schubert, C. J.: Tracing bottom water oxygenation with sedimentary Mn/Fe ratios in Lake Zurich, Switzerland, Chem. Geol., 352, 125-133, https://doi.org/10.1016/j.chemgeo.2013.06.006, 2013.

Nick, F. M., Van Der Veen, C. J., Vieli, A., and Benn, D. I.: A physically based calving model applied to marine outlet glaciers and implications for the glacier dynamics, Journal of Glaciology, 56, 781-794, 10.3189/002214310794457344, 2010.

O'Regan, M., Cronin, T. M., Reilly, B., Alstrup, A. K. O., Gemery, L., Golub, A., Mayer, L. A., Morlighem, M., Moros, M., Munk, O. L., Nilsson, J., Pearce, C., Detlef, H., Stranne, C., Vermassen, F., West, G., and Jakobsson, M.: The Holocene dynamics of Ryder Glacier and ice tongue in north Greenland, The Cryosphere, 15, 4073-4097, 10.5194/tc-15-4073-2021, 2021.

Oppenheimer, M., Glavovic, B., Hinkel, J., van de Wal, R., Magnan, A. K., Abd-Elgawad, A., Cai, R., Cifuentes-Jara, M., Deconto, R. M., and Ghosh, T.: Sea level rise and implications for low lying islands, coasts and communities, 2019.

Pados-Dibattista, T., Pearce, C., Detlef, H., Bendtsen, J., and Seidenkrantz, M. S.: Holocene palaeoceanography of the Northeast Greenland shelf, Clim. Past, 18, 103-127, 10.5194/cp-18-103-2022, 2022.

Palmer, A. P., Bendle, J. M., MacLeod, A., Rose, J., and Thorndycraft, V. R.: The micromorphology of glaciolacustrine varve sediments and their use for reconstructing palaeoglaciological and palaeoenvironmental change, Quat. Sci. Rev., 226, 105964, https://doi.org/10.1016/j.quascirev.2019.105964, 2019.

Perner, K., Moros, M., Lloyd, J. M., Jansen, E., and Stein, R.: Mid to late Holocene strengthening of the East Greenland Current linked to warm subsurface Atlantic water, Quat. Sci. Rev., 129, 296-307, 10.1016/j.quascirev.2015.10.007, 2015.

Perner, K., Moros, M., Lloyd, J. M., Kuijpers, A., Telford, R. J., and Harff, J.: Centennial scale benthic foraminiferal record of late Holocene oceanographic variability in Disko Bugt, West Greenland, Quat. Sci. Rev., 30, 2815-2826, 10.1016/j.quascirev.2011.06.018, 2011.

Porter, C., Morin, P., Howat, I., Noh, M.-J., Bates, B., Peterman, K., Keesey, S., Schlenk, M., Gardiner, J., Tomko, K., Willis, M., Kelleher, C., Cloutier, M., Husby, E., Foga, S., Nakamura, H., Platson, M., Wethington, M., Jr., Williamson, C., Bauer, G., Enos, J., Arnold, G., Kramer, W., Becker, P., Doshi, A., D'Souza, C., Cummens, P., Laurier, F., and Bojesen, M.: ArcticDEM (V1), Harvard Dataverse [dataset], doi:10.7910/DVN/OHHUKH, 2018.

940 Prahl, F. G. and Wakeham, S. G.: Calibration of unsaturation patterns in long-chain ketone compositions for palaeotemperature assessment, Nature, 330, 367-369, 10.1038/330367a0, 1987.

Prahl, F. G., Muehlhausen, L. A., and Zahnle, D. L.: Further evaluation of long-chain alkenones as indicators of paleoceanographic conditions, Geochim. Cosmochim. Acta, 52, 2303-2310, https://doi.org/10.1016/0016-7037(88)90132-9, 1988.

945 Rasmussen, S. O., Abbott, P. M., Blunier, T., Bourne, A. J., Brook, E., Buchardt, S. L., Buizert, C., Chappellaz, J., Clausen, H. B., Cook, E., Dahl-Jensen, D., Davies, S. M., Guillevic, M., Kipfstuhl, S., Laepple, T., Seierstad, I. K., Severinghaus, J. P., Steffensen, J. P., Stowasser, C., Svensson, A., Vallelonga, P., Vinther, B. M., Wilhelms, F., and Winstrup, M.: A first chronology for the North Greenland Eemian Ice Drilling (NEEM) ice core, Clim. Past, 9, 2713-2730, 10.5194/cp-9-2713-2013, 950 2013.

Rasmussen, T. L., Pearce, C., Andresen, K. J., Nielsen, T., and Seidenkrantz, M.-S.: Northeast Greenland: ice-free shelf edge at 79.4°N around the Last Glacial Maximum 25.5–17.5 ka, Boreas, n/a, https://doi.org/10.1111/bor.12593, 2022.

Reimer, P. J., Bard, E., Bayliss, A., Beck, J. W., Blackwell, P. G., Ramsey, C. B., Buck, C. E., Cheng, 955 H., Edwards, R. L., Friedrich, M., Grootes, P. M., Guilderson, T. P., Haflidason, H., Hajdas, I., Hatte, C., Heaton, T. J., Hoffmann, D. L., Hogg, A. G., Hughen, K. A., Kaiser, K. F., Kromer, B., Manning, S. W., Niu, M., Reimer, R. W., Richards, D. A., Scott, E. M., Southon, J. R., Staff, R. A., Turney, C. S. M., and van der Plicht, J.: INTCAL13 AND MARINE13 RADIOCARBON AGE CALIBRATION CURVES 0-50,000 YEARS CAL BP, Radiocarbon, 55, 1869-1887, 10.2458/azu_js_rc.55.16947, 2013.

960 Rieley, G., Collier, R. J., Jones, D. M., Eglinton, G., Eakin, P. A., and Fallick, A. E.: Sources of sedimentary lipids deduced from stable carbon-isotope analyses of individual compounds, Nature, 352, 425-427, 10.1038/352425a0, 1991.

Robel, A. A.: Thinning sea ice weakens buttressing force of iceberg mélange and promotes calving, Nature Communications, 8, 14596, 10.1038/ncomms14596, 2017.

965 Rosell-Melé, A. and McClymont, E. L.: Chapter Eleven Biomarkers as Paleoceanographic Proxies, in: Developments in Marine Geology, edited by: Hillaire–Marcel, C., and De Vernal, A., Elsevier, 441-490, https://doi.org/10.1016/S1572-5480(07)01016-0, 2007.

Sánchez-Montes, M. L., McClymont, E. L., Lloyd, J. M., Müller, J., Cowan, E. A., and Zorzi, C.: Late Pliocene Cordilleran Ice Sheet development with warm northeast Pacific sea surface temperatures, 970 Clim. Past, 16, 299-313, 10.5194/cp-16-299-2020, 2020.

Schaffer, J., Kanzow, T., von Appen, W.-J., von Albedyll, L., Arndt, J. E., and Roberts, D. H.: Bathymetry constrains ocean heat supply to Greenland's largest glacier tongue, Nature Geoscience, 13, 227-231, 10.1038/s41561-019-0529-x, 2020.

975 Seki, A., Tada, R., Kurokawa, S., and Murayama, M.: High-resolution Quaternary record of marine organic carbon content in the hemipelagic sediments of the Japan Sea from bromine counts measured by XRF core scanner, Progress in Earth and Planetary Science, 6, 1, 10.1186/s40645-018-0244-z, 2019.

Seroussi, H., Morlighem, M., Rignot, E., Khazendar, A., Larour, E., and Mouginot, J.: Dependence of century-scale projections of the Greenland ice sheet on its thermal regime, Journal of Glaciology, 59, 1024-1034, 10.3189/2013JoG13J054, 2013.

980 Shepherd, A., Ivins, E., Rignot, E., Smith, B., van den Broeke, M., Velicogna, I., Whitehouse, P., Briggs, K., Joughin, I., Krinner, G., Nowicki, S., Payne, T., Scambos, T., Schlegel, N., A, G., Agosta, C., Ahlstrøm, A., Babonis, G., Barletta, V. R., Bjørk, A. A., Blazquez, A., Bonin, J., Colgan, W., Csatho, B., Cullather, R., Engdahl, M. E., Felikson, D., Fettweis, X., Forsberg, R., Hogg, A. E., Gallee, H., Gardner, A., Gilbert, L., Gourmelen, N., Groh, A., Gunter, B., Hanna, E., Harig, C., Helm, V., Horvath, 985 A., Horwath, M., Khan, S., Kjeldsen, K. K., Konrad, H., Langen, P. L., Lecavalier, B., Loomis, B., Luthcke, S., McMillan, M., Melini, D., Mernild, S., Mohajerani, Y., Moore, P., Mottram, R., Mouginot, J., Moyano, G., Muir, A., Nagler, T., Nield, G., Nilsson, J., Noël, B., Otosaka, I., Pattle, M. E., Peltier, W. R., Pie, N., Rietbroek, R., Rott, H., Sandberg Sørensen, L., Sasgen, I., Save, H., Scheuchl, B., Schrama, E., Schröder, L., Seo, K.-W., Simonsen, S. B., Slater, T., Spada, G., Sutterley, T., Talpe, M., 990 Tarasov, L., van de Berg, W. J., van der Wal, W., van Wessem, M., Vishwakarma, B. D., Wiese, D., Wilton, D., Wagner, T., Wouters, B., Wuite, J., and The, I. T.: Mass balance of the Greenland Ice Sheet from 1992 to 2018, Nature, 579, 233-239, 10.1038/s41586-019-1855-2, 2020.

Slubowska-Wodengen, M., Rasmussen, T. L., Koc, N., Klitgaard-Kristensen, D., Nilsen, F., and Solheim, A.: Advection of Atlantic Water to the western and northern Svalbard shelf since 17,500 cal 995 yr BP, Quat. Sci. Rev., 26, 463-478, 10.1016/j.quascirev.2006.09.009, 2007.

Slubowska, M. A., Koc, N., Rasmussen, T. L., and Klitgaard-Kristensen, D.: Changes in the flow of Atlantic water into the Arctic Ocean since the last deglaciation: Evidence from the northern Svalbard continental margin, 80 degrees N, Paleoceanography, 20, 10.1029/2005pa001141, 2005.

Smith, J. A., Hodgson, D. A., Bentley, M. J., Verleyen, E., Leng, M. J., and Roberts, S. J.: Limnology 1000 of two antarctic epishelf lakes and their potential to record periods of ice shelf loss, J. Paleolimn., 35, 373-394, 10.1007/s10933-005-1333-8, 2006.

Smith, J. A., Bentley, M. J., Hodgson, D. A., Roberts, S. J., Leng, M. J., Lloyd, J. M., Barrett, M. S., Bryant, C., and Sugden, D. E.: Oceanic and atmospheric forcing of early Holocene ice shelf retreat, George VI Ice Shelf, Antarctica Peninsula, Quat. Sci. Rev., 26, 500-516, https://doi.org/10.1016/j.quascirev.2006.05.006, 2007.

Smith, M. P., Higgins, A. K., Soper, N. J., and Sønderholm, M.: The Neoproterozoic Rivieradal Group of Kronprins Christian Land, eastern North Greenland, GEUS Bulletin, 6, 29-39, 10.34194/geusb.v6.4816, 2004a.

Smith, M. P., Rasmussen, J. A., Robertson, S., Higgins, A. K., and Leslie, A. G.: Lower Palaeozoic stratigraphy of the East Greenland Caledonides, GEUS Bulletin, 6, 5-28, 10.34194/geusb.v6.4815, 2004b.

Straneo, F. and Heimbach, P.: North Atlantic warming and the retreat of Greenland's outlet glaciers, Nature, 504, 36-43, 10.1038/nature12854, 2013.

Stuiver, M., Reimer, P. J., and Reimer, R. W.: CALIB 8.1 [WWW program] at http://calib.org, 2021.

Syring, N., Lloyd, J. M., Stein, R., Fahl, K., Roberts, D. H., Callard, L., and O'Cofaigh, C.: Holocene Interactions Between Glacier Retreat, Sea Ice Formation, and Atlantic Water Advection at the Inner Northeast Greenland Continental Shelf, Paleoceanography and Paleoclimatology, 35, e2020PA004019, https://doi.org/10.1029/2020PA004019, 2020.

ten Haven, H. L., de Leeuw, J. W., Sinninghe Damsté, J. S., Schenck, P. A., Palmer, S. E., and Zumberge, J. E.: Application of biological markers in the recognition of palaeohypersaline environments, Geological Society, London, Special Publications, 40, 123, 10.1144/GSL.SP.1988.040.01.11, 1988.

Turton, J. V., Hochreuther, P., Reimann, N., and Blau, M. T.: The distribution and evolution of supraglacial lakes on 79 degrees N Glacier (north-eastern Greenland) and interannual climatic controls, Cryosphere, 15, 3877-3896, 10.5194/tc-15-3877-2021, 2021.

Wagner, B. and Melles, M.: A Holocene seabird record from Raffles Sø sediments, East Greenland, in response to climatic and oceanic changes, Boreas, 30, 228-239, 10.1080/030094801750424148, 2001.

Wagner, B., Melles, M., Hahne, J., Niessen, F., and Hubberten, H. W.: Holocene climate history of Geographical Society Ø, East Greenland — evidence from lake sediments, Paleogeogr. Paleoclimatol. Paleoecol., 160, 45-68, 10.1016/S0031-0182(00)00046-8, 2000.

Walinsky, S. E., Prahl, F. G., Mix, A. C., Finney, B. P., Jaeger, J. M., and Rosen, G. P.: Distribution and composition of organic matter in surface sediments of coastal Southeast Alaska, Cont. Shelf Res., 29, 1565-1579, 10.1016/j.csr.2009.04.006, 2009.

Wang, K. J., Huang, Y., Majaneva, M., Belt, S. T., Liao, S., Novak, J., Kartzinel, T. R., Herbert, T. D., Richter, N., and Cabedo-Sanz, P.: Group 2i Isochrysidales produce characteristic alkenones reflecting sea ice distribution, Nature Communications, 12, 15, 10.1038/s41467-020-20187-z, 2021.

Werner, K., Müller, J., Husum, K., Spielhagen, R. F., Kandiano, E. S., and Polyak, L.: Holocene sea subsurface and surface water masses in the Fram Strait – Comparisons of temperature and sea-ice reconstructions, Quat. Sci. Rev., 147, 194-209, https://doi.org/10.1016/j.quascirev.2015.09.007, 2016.

Winkelmann, D., Jokat, W., Jensen, L., and Schenke, H.-W.: Submarine end moraines on the continental shelf off NE Greenland – Implications for Lateglacial dynamics, Quat. Sci. Rev., 29, 1069-1077, https://doi.org/10.1016/j.quascirev.2010.02.002, 2010.

Winnell, M. H. and White, D. S.: The Distribution of Heterotrissocladius-Oliveri Saether (Diptera, Chironomidae) in Lake-Michigan, Hydrobiologia, 131, 205-214, Doi 10.1007/Bf00008856, 1986.

Wollenburg, J. E. and Mackensen, A.: Vertical distribution of benthic foraminifers in the Arctic Ocean, 10.1594/PANGAEA.712695, 1998.

Wood, M., Rignot, E., Fenty, I., An, L., Bjørk, A., Broeke, M. v. d., Cai, C., Kane, E., Menemenlis, D., Millan, R., Morlighem, M., Mouginot, J., Noël, B., Scheuchl, B., Velicogna, I., Willis, J. K., and Zhang, H.: Ocean forcing drives glacier retreat in Greenland, Science Advances, 7, eaba7282, doi:10.1126/sciadv.aba7282, 2021.

Yin, J., Overpeck, J. T., Griffies, S. M., Hu, A., Russell, J. L., and Stouffer, R. J.: Different magnitudes of projected subsurface ocean warming around Greenland and Antarctica, Nature Geoscience, 4, 524-528, 10.1038/ngeo1189, 2011.

Ziegler, M., Jilbert, T., de lange, G. J., Lourens, L. J., and Reichart, G.-J.: Bromine counts from XRF scanning as an estimate of the marine organic carbon content of sediment cores, Geochem. Geophys. Geosyst., 9, 10.1029/2007gc001932, 2008.
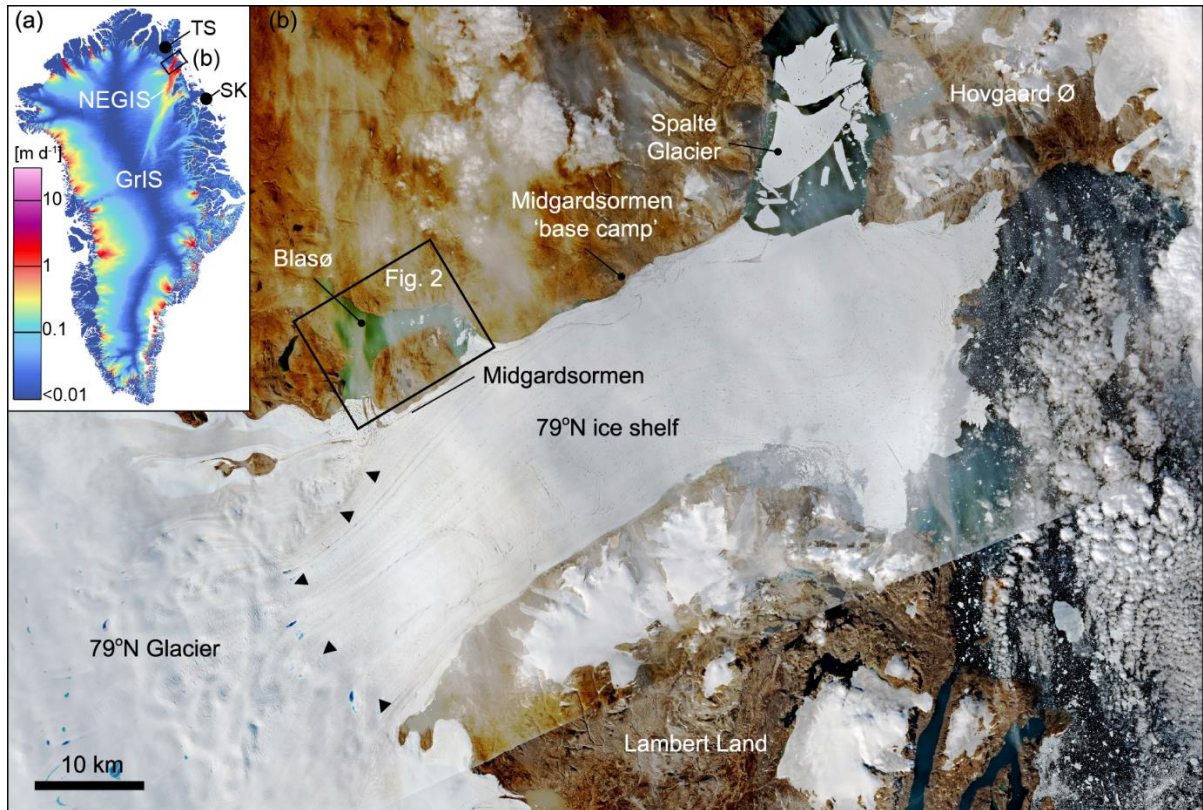
Figure 1. (a) Ice velocity map of the Greenland Ice Sheet (GrIS) (Mottram et al., 2019), showing the location of the North East Greenland Ice Stream (NEGIS) and the study area (b), Trifna Sø (TS) and Store Koldeway/Duck Lake (SK); **(b)** Sentinel-2 L2A imagery of 79°N Glacier and its floating ice shelf. Contains modified Copernicus Sentinel data August, 2020) processed by the Sentinel Hub EO Browser (https://www.sentinel-hub.com/). Blåsø is located 2-13 km from the grounding line (GL) of 79°N Glacier, delineated by black triangles. The remnants of Spalte Glacier, a northern tributary of 79°N Glacier which broke up in 2020, is also shown.
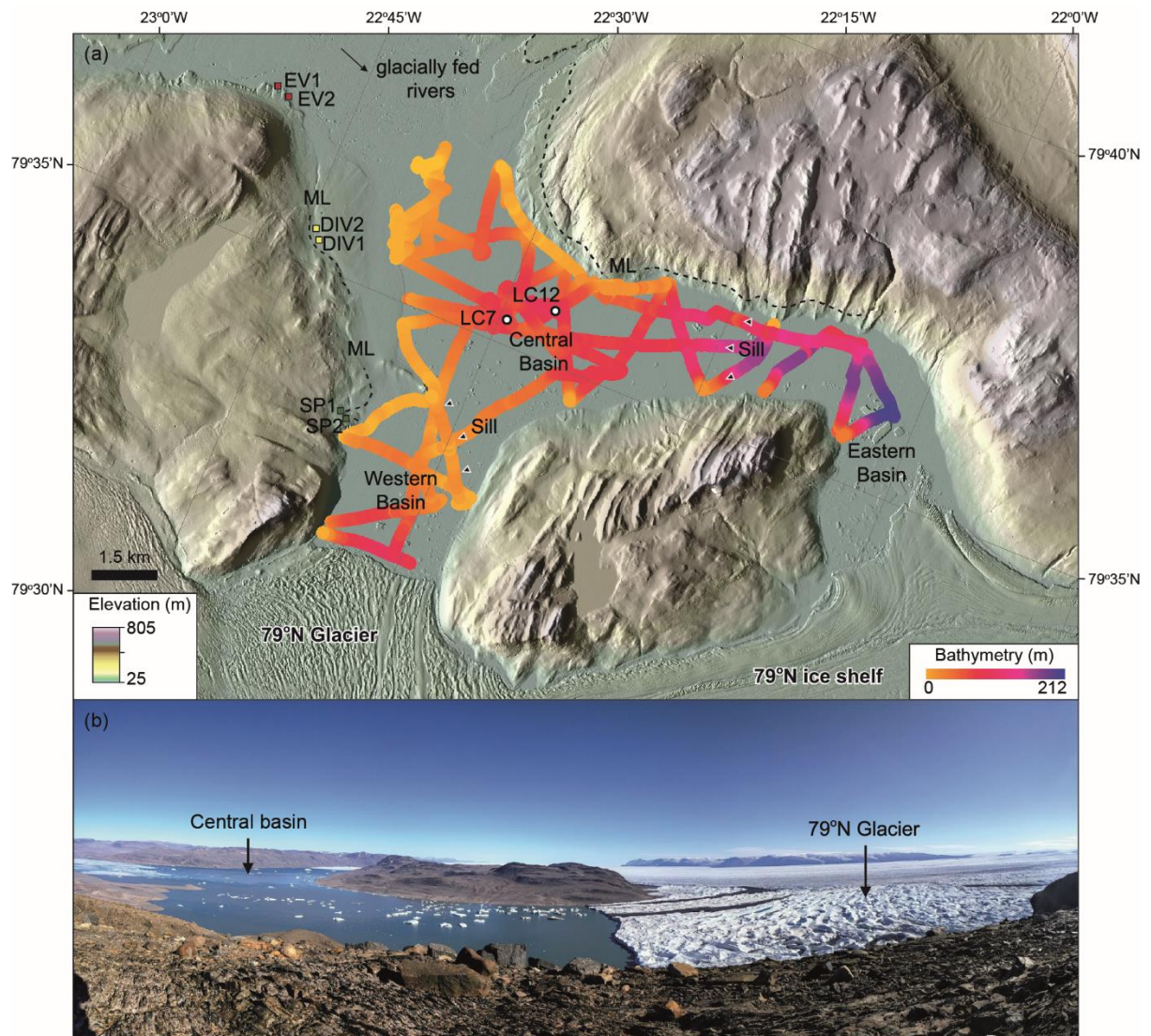
Figure 2. (a) Bathymetry of Blåsø showing the locations of sediment cores LC7 and LC12 as well as the western, central and eastern basins. The bathymetry is overlain by the ArticDEM (Porter et al., 2018). The central basin is currently isolated from marine water by shallow sills (black triangles) at the margins of the western and eastern basins. Also shown are the location of uplifted glacimarine sediments (SP1-2, DIV1-2, EV1-2) and location of glacially-fed rivers entering the basin. Black dashed lines delineates the marine limit (ML); **(b)** Photograph of Blåsø looking east. 79°N Glacier is shown in the foreground (right of frame) together with the approximate location of the central basin. Author photograph (DHR).
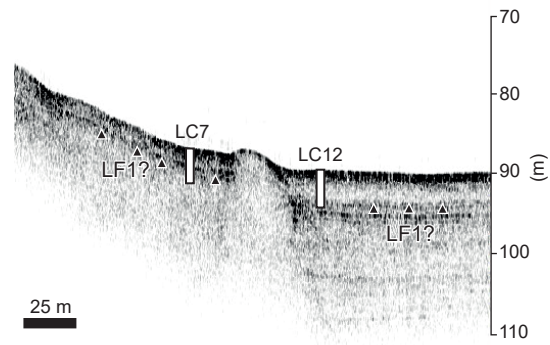
Figure 3. Sub-bottom profile across coring site LC7 and LC12, in the central basin of Blåsø. The prominent reflector ~3-4 m below lake-floor likely relates to deposition of lithofacies (LF) 1 during ice shelf retreat.
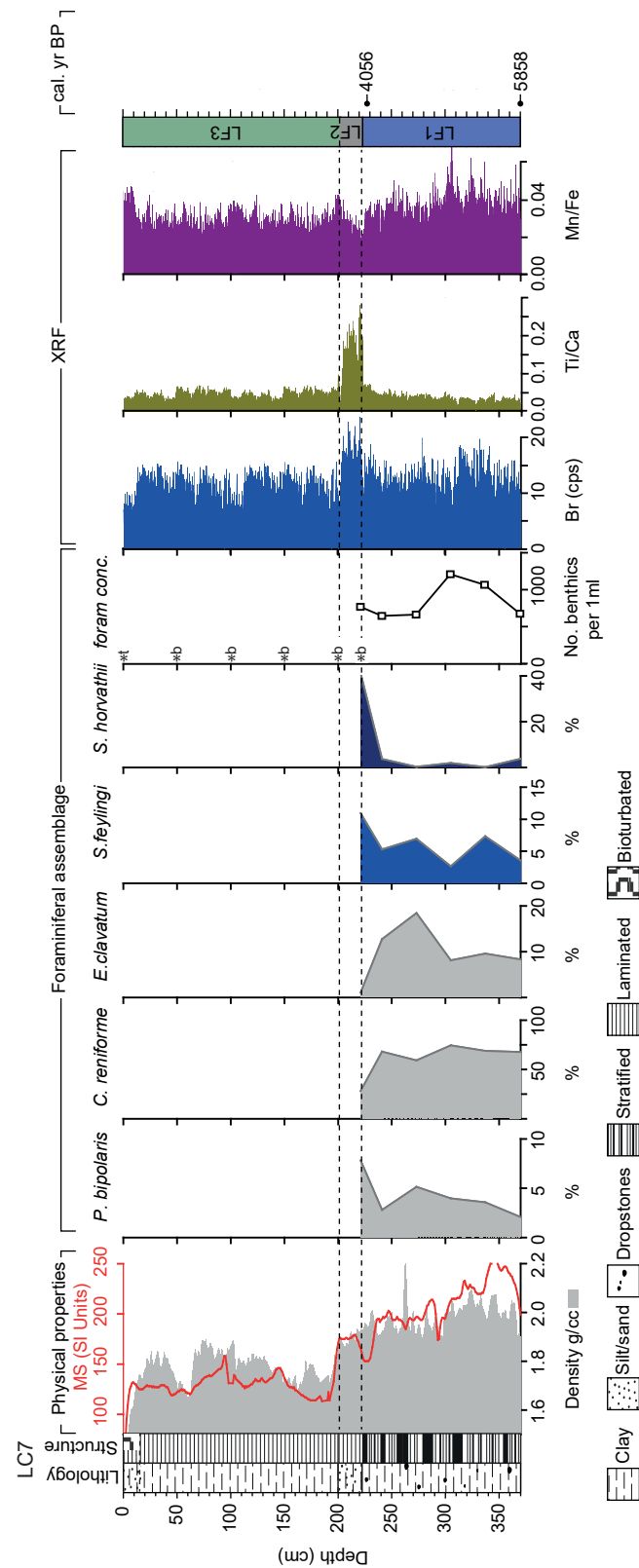
Figure 4. Multi-proxy data for core LC7, including simplified core lithology/structure, physical properties (magnetic susceptibility (MS), density), foraminiferal assemblage data (b=barren, t=trace (<20) foram) and selected XRF-scanner data. Horizontal (dashed) lines delineate the main lithofacies (LF) 1-3. Calibrated ages are also shown.
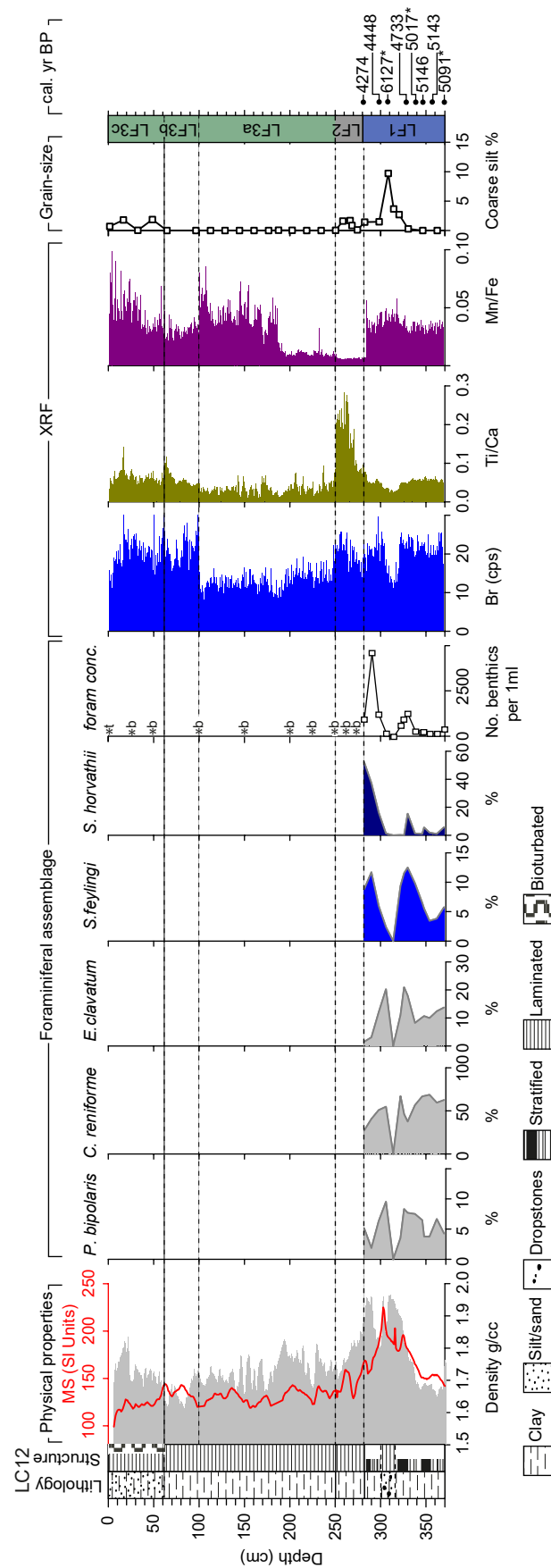
Figure 5. Multi-proxy data for core LC12, including simplified core lithology/structure, physical properties (magnetic susceptibility (MS), density), foraminiferal assemblage data (b=barren, t=trace (<20) foram), selected XRF-scanner and grain-size (coarse silt) data. Horizontal (dashed) lines delineate the main lithofacies (LF) 1-3. Calibrated ages are also shown. *Denotes age-reversals.
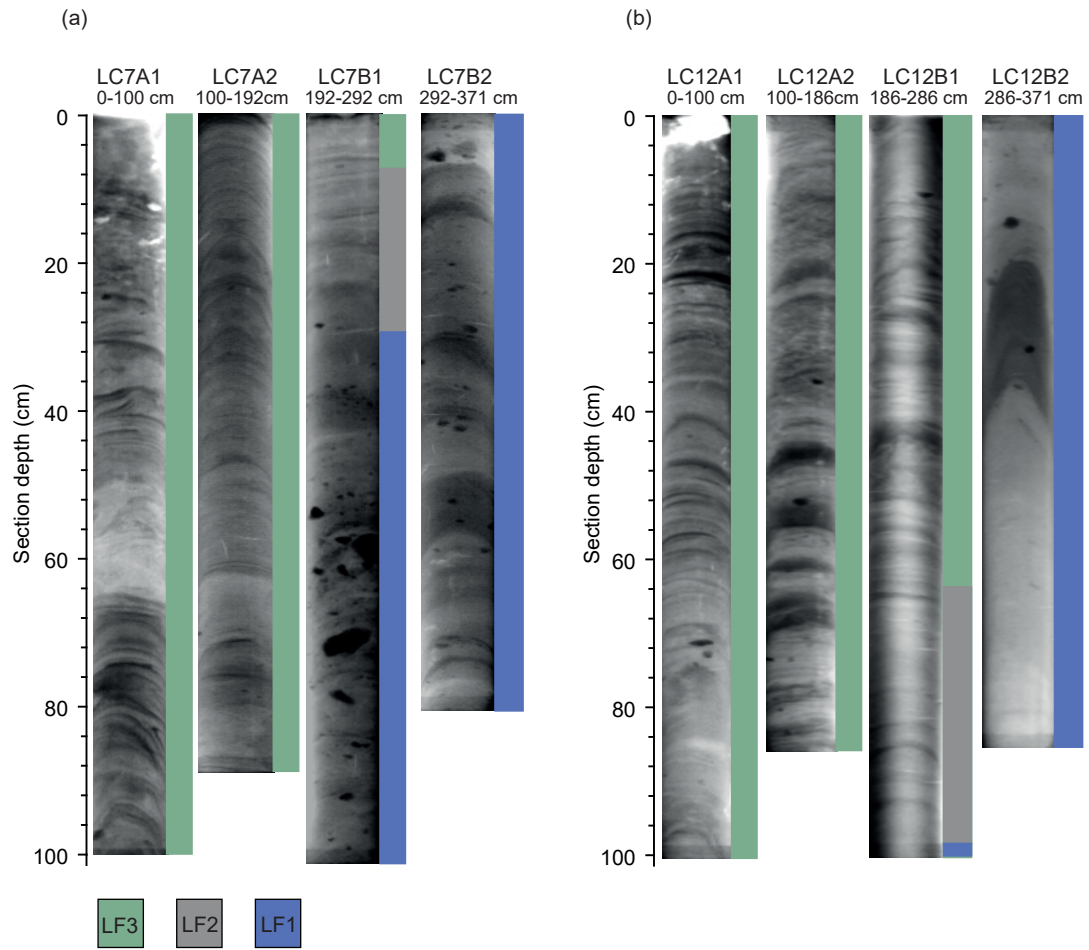
Figure 6. X-radiographs of (a) LC7 and (b) LC12 together with associated lithofacies (LF) 1-3.
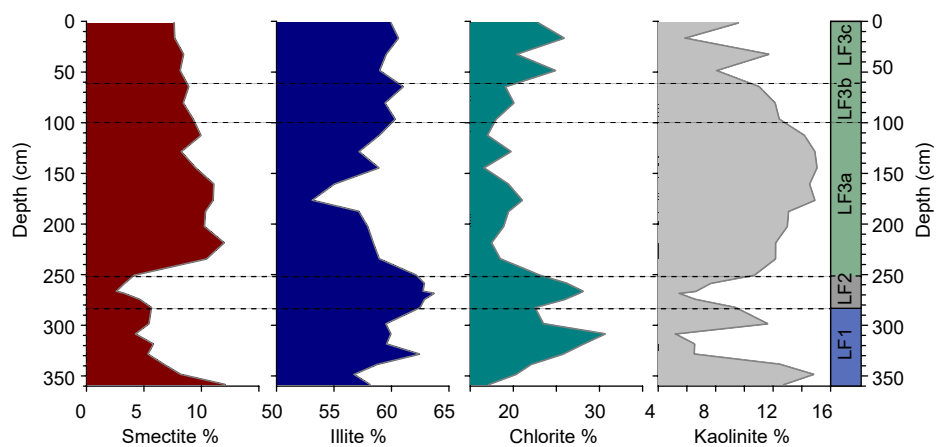
Figure 7. Clay mineral assemblage data for LC12. Horizontal (dashed) lines delineate the main lithofacies (LF) 1-3.
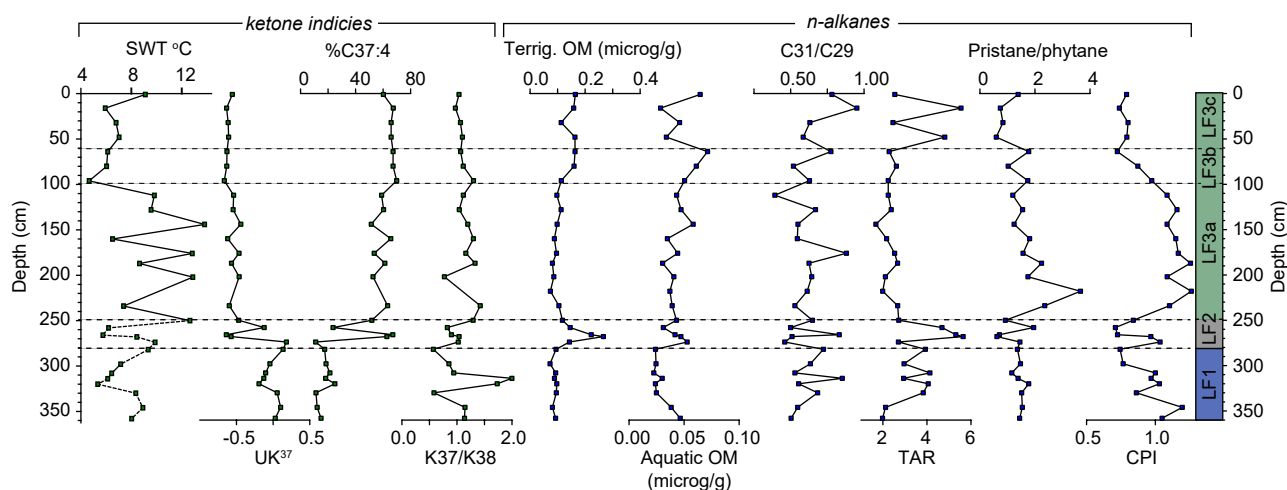
Figure 8. Biomarker (n-alkanes, ketone indices) data for LC12. Horizontal (dashed) lines delineate the main lithofacies (LF) 1-3. Surface water temperature (SWT) was calculated using both D'Andrea et al. (2011) (LF3 - solid line) and Bendle and Rosell-Melé (2004) (LF1 & LF2 - dashed line) for the 'lake' and 'marine' phases respectively.
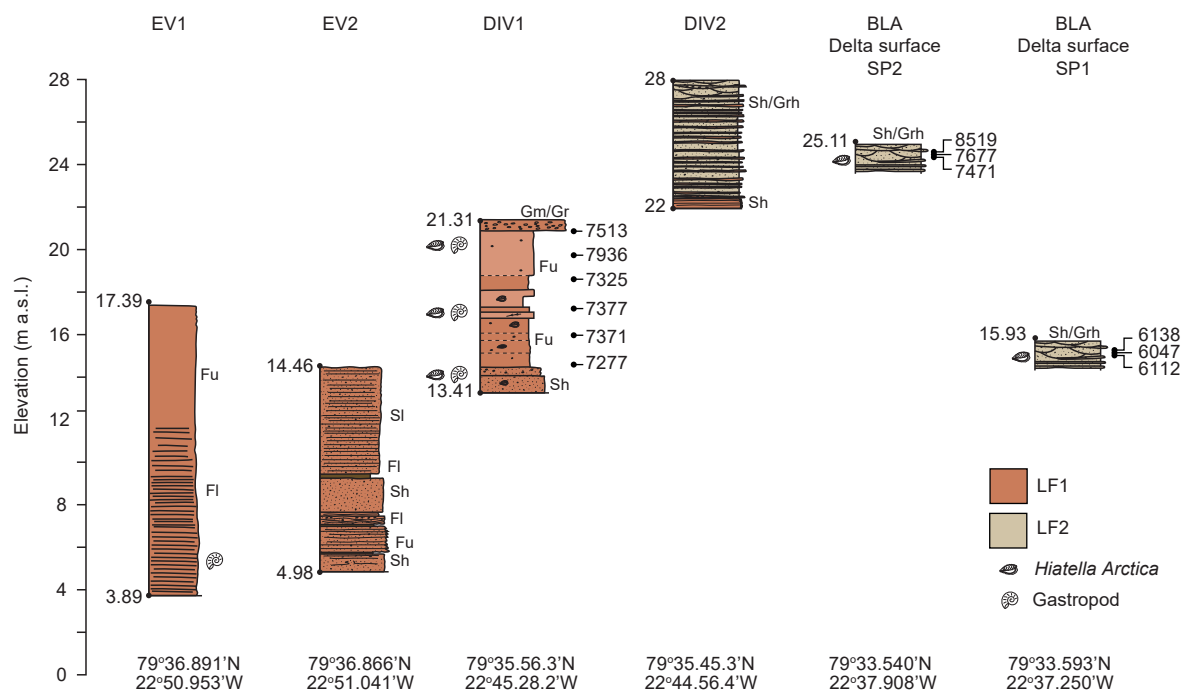
Figure 9. Altitudinal profile of the Blåsø uplifted glacimarine and deltaic sediments (BUG). Gm = massive/crudely bedded gravel =, Grh = horizontally bedded gravel, Gr = gravel, ripple-cross laminated, Sh = sheared/laminated sand, Fu = upward fining mud, =, Fl = laminated mud/sand, Sl = cross-bedded sand. Radiocarbon ages (cal. yr. BP) are shown to the right of section logs.
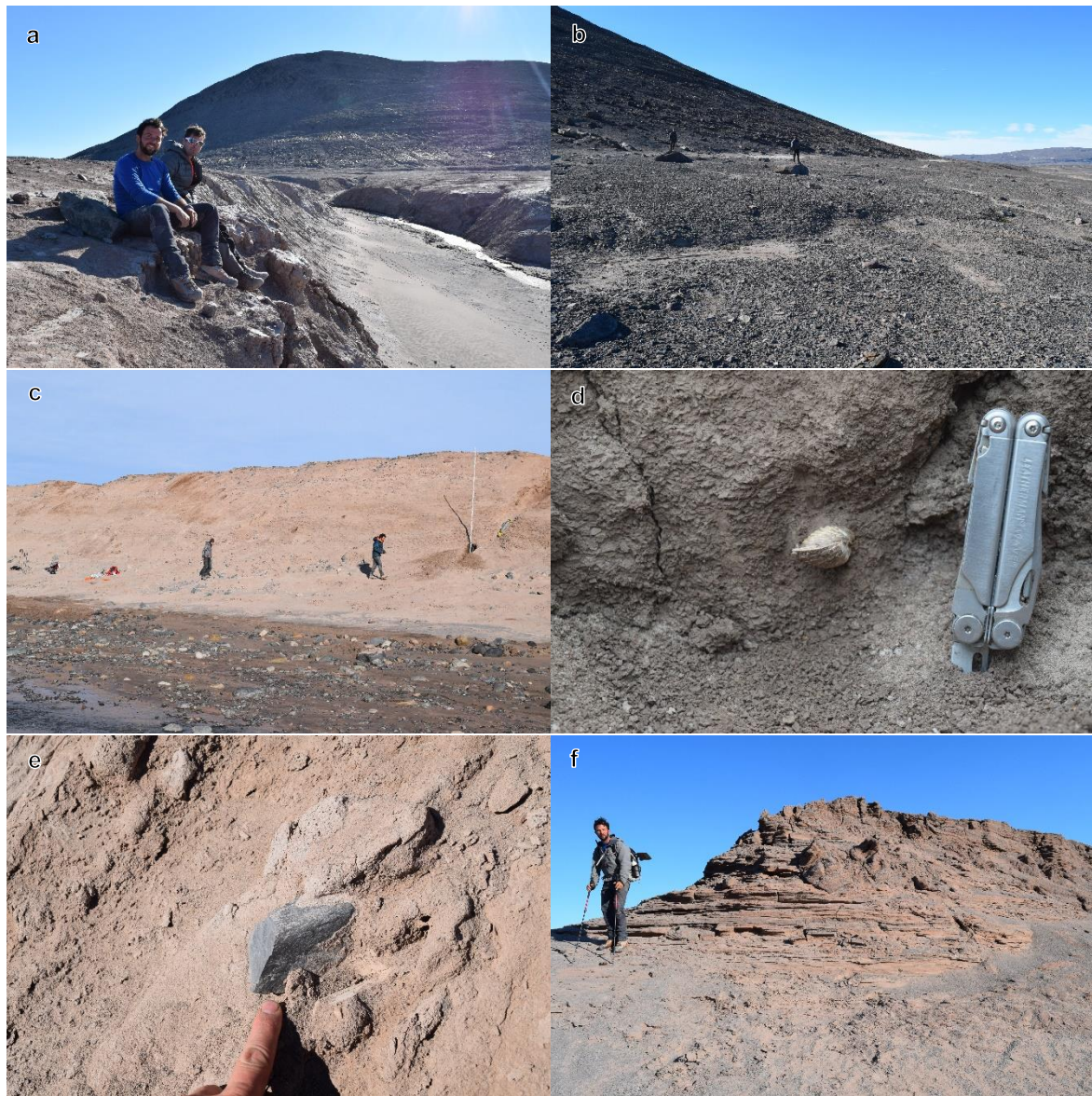
Figure 10. Photos of Blåsø uplifted glacimarine (BUG) and deltaic sediments. **(a)** Uplifted glacimarine sediments peripheral to Blåsø at site EV1. The marine limit at ~ 33 m.a.s.l can be seen in the background. Below this, lithofacies BUG/LF1 is exposed due to local stream incision; **(b)** The marine limit at ~ 33 m.a.s.l. close to site EV1; **(c)** Lithofacies BUG/LF1 sediments exposed at site DIV 1. These are predominantly massive to partially stratified red clay/silts with an assemblage of paired molluscs. They are capped by a thin layer of gravel; **(d)** A paired *Hiatella arctica* valve within lithofacies BUG/LF1 at site DIV1; **(e)** A striated, dropstone in lithofacies BUG/LF1 indicating an ice-rafted component within this lithofacies; **(f)** Lithofacies BUG/LF2 exposed at site DIV2 at 28 m.a.s.l. This lithofacies varies in elevation, but is characterised by planar and trough cross-bedded sand and gravels that often from distinctive flat surfaces peripheral to the Blåsø shoreline. Author photographs (DHR).
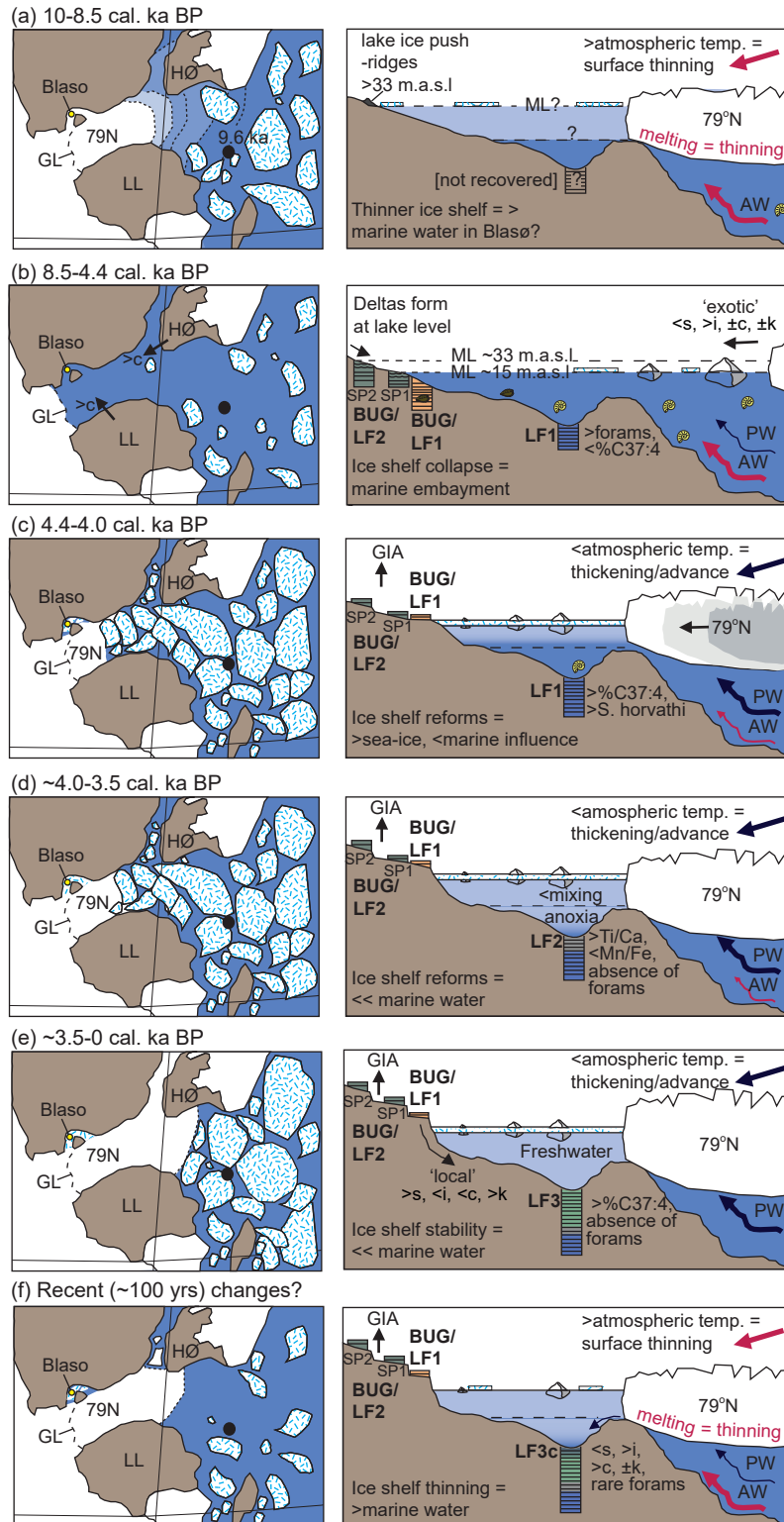
Figure 11. Reconstruction of 79°N ice shelf from 10 ka cal. BP to present, showing location of Blåsø, Lambert Land (LL) and Hovgaard Ø (HØ). Constraints on sea ice (blue-hatched polygons) formation and ocean circulation on the adjacent continental shelf (left panel) are derived from core PS100/270 (closed black circle; Syring et al., 2020). Relative proportions of Atlantic Water (AW) and Polar Water (PW) are shown as thick/thin arrows. Conditions in Blåsø catchment (right panel) prior to 8.5 cal. ka BP (youngest shell age) are inferred. Relative proportions (>=high, <=low, and ±=variable) inferred pathways of smectite (s), illite (i), chlorite (c), kaolinite (k) are indicated, together with key attributes of lithofacies (LF) 1-3 in lakes cores and Blåsø uplifted (BUG) lithofacies. Paler blue shading indicates more brackish/fresh water in Blåsø. ML = marine limit, GIA = glacial isostatic adjustment. Yellow star in Blåsø (left panels) shows relative position of cores LC7 and LC12.
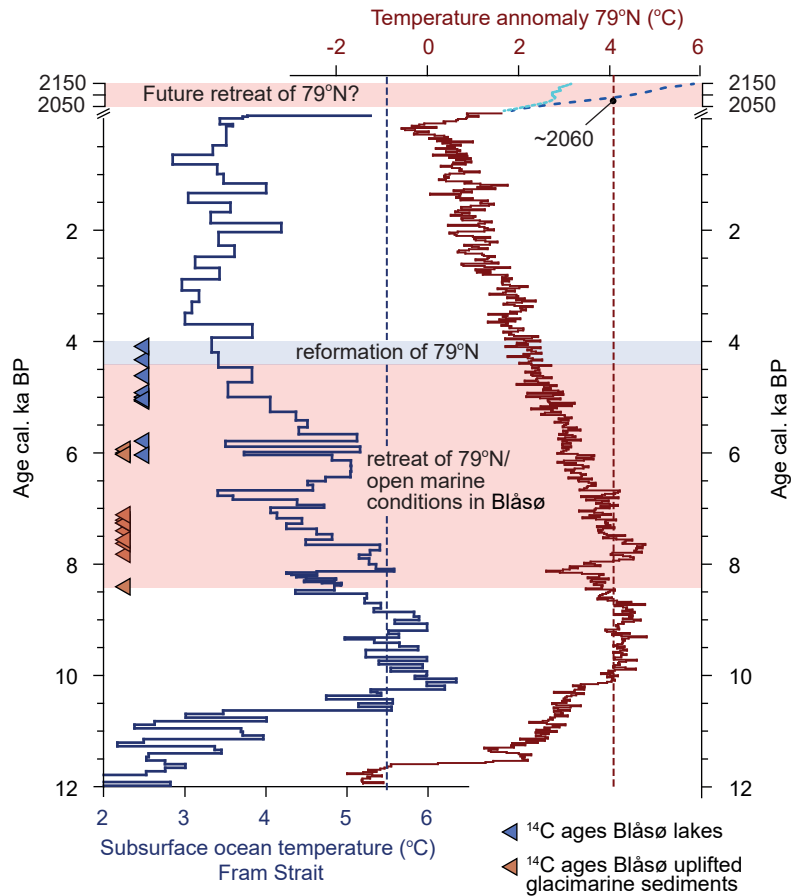
Figure 12. Marine conditions in Blåsø vs. atmospheric and ocean temperature. Ice shelf retreat (red shading) and reformation (blue shading) is constrained by ^{14}C ages (cal. ka BP) on shells samples from uplifted glacimarine sediments (brown triangles) and foraminiferal samples from LC12 and LC7 (light blue triangles) in Blåsø. Subsurface ocean temperatures derived from planktic foraminiferal fauna assemblages (SST100) from core MSM5/5-723-2 (blue curve) (Werner et al., 2016). Summer temperature (JJA) (red curve) at 79°N based on data-model outputs (Buizert et al., 2018). Also shown are Representative Concentration Pathway (RCP) 2.6 (light blue dotted line) and 8.5 scenarios (dark blue dashed line) (Hofer et al., 2020). Vertical dashed lines denote mean ocean (blue) and atmosphere (red) temperatures for the Early Holocene ~10-8 ka. Under RCP8.5 (red shading), comparable Early Holocene atmosphere and ocean temperatures could occur by 2060.

Fraction	Equations	Interpretation	References
Ketone	$U_{37}^K = \dfrac{[C_{37:2}] - [C_{37:4}]}{[C_{37:2}] + [C_{37:3}] + [C_{37:4}]}$	Surface water temperature and salinity.	Prahl and Wakeham, (1987).
Ketone	$\%C_{37:4} = \dfrac{[C_{37:4}]}{[C_{37:2}]+[C_{37:3}]+[C_{37:4}]} *100$	Surface water temperature and salinity.	Bendle and Rosell-Melé, (2004(.
Ketone	$K_{37}/ K_{38} = \dfrac{\sum[C_{37}]}{\sum[C_{38}]}$	Changes in Haptophyceae species producing alkenones.	Prahl et al., (1988).
Ketone	$U_{37}^K = \dfrac{SWT-31.8}{40.8}$ r^2=0.96 and n=34	Freshwater surface water temperature calibration.	D'Andrea et al. (2011).
Ketone	$U_{37}^K = 0.082\ SWT - 0.63$	Marine surface water temperature calibration.	Bendle and Rosell-Melé, (2004).
Ketone	$APE = \dfrac{mass\ 2nonadecanone}{[2nonadecanone]} * [C_{37}A]$	Haptophyceae productivity export.	Prahl et al., (1988); Rosell-Melé and McClymont, (2007).
n-alkane	Terrigenous OM $= [C_{27}] + [C_{29}] + [C_{31}]$	Terrigenous organic matter from higher plants.	Rieley et al., (1991).
n-alkane	Aquatic OM $= [C_{15}] + [C_{17}] + [C_{19}]$	Aquatic productivity export of bacteria and phytoplankton.	Cranwell, (1973).
n-alkane	$CPI = \dfrac{\dfrac{[C25-33(odd)]}{[C24-32(even)]} + \dfrac{[C25-33(odd)]}{[C26-34(even)]}}{2}$	Sediment maturity.	Bray and Evans, (1961).
n-alkane	$Pristane/Phytane = \dfrac{[Pristane]}{[Phytane]}$	Relative oxidative or reductive conditions, sediment maturity.	Ten Haven et al., (1988); Bray and Evans, (1961).
n-alkane	$C_{31}/C_{29} = \dfrac{[C_{31}]}{[C_{29}]}$	Relative grassy or woody vegetation contribution.	Guillemot et al., (2017).
n-alkane	$TAR = \dfrac{[C27] + [C29] + [C31]}{[C15] + [C17] + [C19]}$	Relative terrestrial and aquatic contributions.	Cranwell, (1973).

Table 1. Summary of lipid biomarker proxies analysed.

Publication code	Sample ID	Depth (cm)	Material	Lithofacies	δ¹³CVPDB‰ ± 0.1	¹⁴C Age (¹⁴C yrs BP)	±	ΔR	±	Calibrated age (cal. yr BP) Min	Max	Mean
SUERC-90493	SC9	0	AIOM	LF3	-28.926	17259	75	0	0	-	-	-
UCIAMS-211060	LC7	229	Mixed bf	LF1		4170	30	0	0	3881	4230	4056
BETA-499519	LC7	378.5	Mixed bf	LF1		5670	30	0	0	5690	6025	5858
SUERC-90494	LC7	202.5	AIOM	LF1	-29.902	15211	63	0	0	-	-	-
UCIAMS-216429	LC12	279	Mixed bf	LF1		4345	30	0	0	4100	4447	4274
UCIAMS-216430	LC12	371	Mixed bf	LF1		4970	25	0	0	4858	5293	5076
SUERC-90482	LC12	11	AIOM	LF3c	-28.459	11593	45	0	0	-	-	-
SUERC-90483	LC12	94.5	AIOM	LF3b	-28.174	18388	85	0	0	-	-	-
SUERC-90484	LC12	183	AIOM	LF3a	-28.046	22367	133	0	0	-	-	-
SUERC-90489	LC12	246	AIOM	LF3a	-28.554	15864	65	0	0	-	-	-
SUERC-90490	LC12	263	AIOM	LF2	-27.864	11156	45	0	0	-	-	-
SUERC-90491	LC12	297	AIOM	LF1	-27.005	12074	47	0	0	-	-	-
SUERC-90492	LC12	326.5	AIOM	LF1	-28.047	14011	55	0	0	-	-	-
UCIAMS-223836	LC12	307	Mixed bf	LF1		5910	30	0	0	5919	6302	6111
UCIAMS-223837	LC12	337	Mixed bf	LF1		4895	40	0	0	4789	5260	5025
UCIAMS-223840	LC12	347	Mixed bf	LF1		5035	35	0	0	4911	5399	5155
UCIAMS-225387	LC12	297	Mixed bf	LF1		4465	25	0	0	4209	4696	4453
UCIAMS-225388	LC12	327	Mixed bf	LF1		4705	25	0	0	4514	4961	4738
UCIAMS-225389	LC12	357	Mixed bf	LF1		5025	25	0	0	4892	5362	5127
SUERC-86006	Neg_Blaso_DIV_Sh01	-	Hiatella Arctica	BUG/LF1	1.573	7168	38	0	0	7282	7634	7458
SUERC-86007	Neg_Blaso_DIV_Sh02	-	Hiatella Arctica	BUG/LF1	0.695	7117	35	0	0	7241	7584	7413
SUERC-86008	Neg_Blaso_DIV_Sh03	-	Hiatella Arctica	BUG/LF1	1.555	6958	36	0	0	7068	7452	7260
SUERC-86009	Neg_Blaso_DIV_Sh05	-	Hiatella Arctica	BUG/LF1	0.621	7019	35	0	0	7147	7505	7326
SUERC-86013	Neg_Blaso_DIV_Sh013	-	Hiatella Arctica	BUG/LF1	1.463	7012	35	0	0	7142	7502	7322
SUERC-86014	Neg_Blaso_DIV_Sh015	-	Hiatella Arctica	BUG/LF1	1.395	6845	37	0	0	6937	7351	7144
UCIAMS-216453	Neg_Blaso_Delta_SP2A	-	Gastropod/bivalve	BUG/LF2		7420	50	0	0	7511	7904	7708
UCIAMS-216454	Neg_Blaso_Delta_SP2B	-	Gastropod/bivalve	BUG/LF2		7345	40	0	0	7442	7814	7628
SUERC-86015	Neg_Blaso_Delta_SP2C	-	Gastropod/bivalve	BUG/LF2	-0.538	8205	35	0	0	8320	8758	8539
SUERC-86016	Neg_Blaso_Delta_SP1A	-	Gastropod/bivalve	BUG/LF2	-0.272	5858	36	0	0	5885	6273	6079
SUERC-86017	Neg_Blaso_Delta_SP1B	-	Gastropod/bivalve	BUG/LF2	0.53	5794	37	0	0	5782	6214	5998
SUERC-86018	Neg_Blaso_Delta_SP1C	-	Gastropod/bivalve	BUG/LF2	-0.394	5900	38	0	0	5908	6298	6103

Table 2. Compilation of radiocarbon (¹⁴C) ages for cores LC7 and LC12 and uplifted glacimarine sediments. Bf = benthic and AIOM = acid insoluble organic matter. All ¹⁴C-ages were corrected using a marine reservoir effect (MRE) of ~550 years (ΔR of 0±0 years) following Hansen et al. (2022). Corrected ¹⁴C-ages were calibrated with the CALIB Radiocarbon Calibration Program version 8.1.0 (http://calib.qub.ac.uk/calib/) using the Marine20 calibration curve (Heaton et al., 2020). Calibrated ages are given as a 2σ range (min, max and mean).